

AD No. \_\_\_\_\_  
DDC FILE COPY

AD A 056795

LEVEL

12

JUL 28 1978

F

Unclassified

SECURITY CLASSIFICATION OF THIS PAGE (When Data Entered)

19 REPORT DOCUMENTATION PAGE		READ INSTRUCTIONS BEFORE COMPLETING FORM
1. REPORT NUMBER NSWC/DL TR-3838	2. GOVT ACCESSION NO.	3. RECIPIENT'S CATALOG NUMBER
4. TITLE (and Subtitle) IMPROVED TRANSONIC NOSE DRAG ESTIMATES FOR THE NSWC MISSILE AERODYNAMIC COMPUTER PROGRAM.		5. TYPE OF REPORT & PERIOD COVERED Contractor Report 3/4/77 - 10/4/77
6. AUTHOR(s) Denny S. Chaussee	7. PERFORMING ORG. REPORT NUMBER NEAR-TR-153	8. CONTRACT OR GRANT NUMBER(s) N60921-77-C-A085
9. PERFORMING ORGANIZATION NAME AND ADDRESS Nielsen Engineering & Research, Inc. 510 Clyde Avenue Mountain View, CA 94043		10. PROGRAM ELEMENT, PROJECT, TASK AREA & WORK UNIT NUMBERS Apr 78
11. CONTROLLING OFFICE NAME AND ADDRESS Naval Surface Weapons Center (K21) Dahlgren Laboratory Dahlgren, Virginia 22448		12. REPORT DATE November 1977
13. MONITORING AGENCY NAME & ADDRESS (if different from Controlling Office) Technical rept. 4 Mar - 4 Oct 78		13. NUMBER OF PAGES 73
		14. SECURITY CLASS. (of this report) Unclassified
15. DISTRIBUTION STATEMENT (of this Report) Approved for public release - distribution unlimited.		15a. DECLASSIFICATION/DOWNGRADING SCHEDULE NA
16. DISTRIBUTION STATEMENT (of the abstract entered in Block 20, if different from Report) F32399, SR02302		
17. SUPPLEMENTARY NOTES SF32399592, SR02302001		
18. KEY WORDS (Continue on reverse side if necessary and identify by block number) Transonic Flow Computational Fluid Dynamics Sphere-ogive-cylinder Configuration Inviscid Nose Drag		
19. ABSTRACT (Continue on reverse side if necessary and identify by block number) An axisymmetric implicit unsteady Euler equation solver has been applied to the transonic flow past sphere-ogive-cylinder bodies. This paper documents this method and shows results that were obtained for the full range of transonic Mach numbers, 0.7 to 1.2. The present numerical results are compared to the experiments of Hsieh for $M_\infty = 0.7, 0.95, 1.0, 1.05, 1.1$ flow over hemisphere cylinders. A rather extensive parametric study		

DD FORM 1 JAN 73 1473

EDITION OF 1 NOV 65 IS OBSOLETE

Unclassified

SECURITY CLASSIFICATION OF THIS PAGE (When Data Entered)

389 783 78

07

21

act

Unclassified

SECURITY CLASSIFICATION OF THIS PAGE(When Data Entered)

of sphere-ogive-cylinders was performed over the transonic Mach number range. Nose pressure drag values were calculated and are presented for varying nose radii, 0 to 1.0, varying nose length, 1.0 to 10.0 and varying Mach numbers, 0.7 to 1.2, where all geometric quantities are normalized with respect to the maximum body radius. These results have been included in the NSWC Missile Aerodynamic Computer program to improve transonic nose drag estimates.

Unclassified

SECURITY CLASSIFICATION OF THIS PAGE(When Data Entered)



## FOREWORD

This technical report covers the work performed under Contract N60921-77-C-A085 from 4 March 1977 to 4 October 1977. The program is sponsored by the Naval Surface Weapons Center, Dahlgren Laboratory (NSWC/DL), Dahlgren, Virginia.

The funding support was provided by the Naval Sea Systems Command (NAVSEA) SEATASKs SF 32399-592/18450 and SR02302-001-18635, Naval Air Systems Command (NAVAIR) NIF, and Army Missile Research and Development Command, Research Element No. 62303A.

This report was reviewed for technical accuracy by Dr. J. Sun and Dr. L. Devan and approved by Dr. F. G. Moore, Head, Aeromechanics Branch and H. P. Caster, Head, Exterior Ballistics Division.

Released by:

Boyd A. Newman

R. A. NIEMANN, Head  
Strategic Systems Department

Accession for [ ] Section [ ]  
[ ] Section [ ]

NTIS  
DDC  
UNANNOUENCED  
JUSTIFICATION

BY DISTRIBUTION/AVAILABILITY CODES  
Dist.

A



#### ACKNOWLEDGMENT

The author would like to express his appreciation to Dr. P. Kutler, Dr. T. Pulliam, both of NASA/Ames and to Dr. M. Hemsch of NEAR, Inc. for their consultation and helpful suggestions during this study and to the Computational Fluid Dynamics Branch at NASA/Ames Research Center, Moffett Field, California, for the allocation of computer time throughout the study.

This technical report covers the work performed under Contract N60921-77-C-A085 from 4 March 1977 to 4 October 1977. The program is sponsored by the Naval Surface Weapons Center, Dahlgren Laboratory (NSWC/DL), Dahlgren, Virginia.

Dr. J. Sun and Dr. L. Devan, Dahlgren Laboratory were the contract monitors for this study.

## CONTENTS

	<u>Page</u>
INTRODUCTION	1
ANALYSIS	2
Implicit Unsteady Euler Equation Method	2
Drag Calculation	8
Body Geometry	10
Table Lookup Method	12
RESULTS AND DISCUSSION	13
Comparison of Pressure Prediction Methods	13
Drag Predictions and Comparisons	26
Computer Program Alterations	42
CONCLUSIONS AND RECOMMENDATIONS	43
REFERENCES	50
GLOSSARY OF TERMS	52
DISTRIBUTION	

# LIST OF ILLUSTRATIONS

<u>Figure</u>		<u>Page</u>
1	Transformation of Physical Plane to Computational Plane for a Single Solver. . . . .	4
2	Nomenclature for Drag Calculation. . . . .	9
3	Ogive Body Geometry Definition . . . . .	11
4	Typical Example of Computational Grid. . . . .	14
5	Pressure Distribution on Hemisphere-Cylinder . . . . .	16
6	Hemisphere-Cylinder Drag Variation with $M_\infty$ . . . . .	18
7	Embedded Supersonic Region at $M_\infty = 0.95$ for Flow Over a Hemisphere Cylinder . . . . .	19
8	Comparison of Theoretical and Experimental Location of Shock Angle for $M_\infty = 1.1$ for Flow Over a Hemisphere Cylinder . . . . .	20
9	Shock Wave and Sonic Line Location for $M_\infty = 1.1$ Flow Over a Hemisphere Cylinder . . . . .	21
10	Evolution of Drag Solution for Hemisphere Cylinder . . . . .	22
11	Comparison Between Experiment and Theory for $M_\infty = 0.95$ Flow Past a 4 Caliber Tangent Ogive Body . . . . .	23
12	Calculated Body Pressure on Sphere-Ogive-Cylinders for Varying Nose Bluntnesses, Nose Lengths, and Mach Numbers. . . . .	24
13	Calculated Values of Nose Pressure Drag Presented as a Function of Nose Length and Nose Bluntness for Varying Mach Numbers . . . . .	29
14	Transonic Wave Drag of Pointed Tangent Ogives for Various Nose Lengths in Calibers . . . . .	33
15	Total and Forebody Drag Comparisons of the Present and Previous Theoretical Results with Experiment . . . . .	35
16	Total and Forebody Drag Comparisons of the Present and Previous Theoretical Results with Experiment . . . . .	37
17	Total and Forebody Drag Comparisons of the Present and Previous Theoretical Results with Experiment . . . . .	39
18	Sample Input Data for a Typical Tangent Ogive Configuration. . . . .	47
19	Sample Output for Tangent Ogive Configuration of Figure 18. . . . .	48



## INTRODUCTION

Accurate drag predictions are essential for optimum missile design. For Mach numbers in the transonic regime, the NSWC code<sup>1</sup> is currently applicable to missiles with pointed or slightly blunted noses. This restriction results from the use of methods based on small perturbation theory such as Wu and Aoyoma.<sup>2</sup> When bluntness effects become large, it is necessary to account for radial flow velocities comparable to free stream velocities over a sizable region of the flow field. A fundamental failing of small-disturbance theory is that it cannot do this.

A precise calculation of nose wave drag depends upon the accurate determination of surface pressures both in the stagnation region and the shoulder region. This is because the overpressure in the stagnation region creates a large drag force which is partially or wholly counterbalanced by the flow expansion in the shoulder region. In subsonic flows, the balance is exact for the nose itself, while in transonic flows, one is attempting to find the difference of two large, nearly equal quantities in order to compute the nose wave drag. Consequently, a method is required which can maintain the required accuracy in these regions.

The computation of nose wave drag, then, for the transonic speed range requires an accurate code capable of properly treating the inviscid flow physics. The exact governing equations are the Euler equations. In the present report an implicit Euler equation solver<sup>3,4,5</sup> is used to calculate the flow field around the bodies and pressures on the bodies. These pressures are then integrated to obtain the nose drag coefficient for a set of Mach numbers, nose bluntnesses and nose lengths. The resulting table of transonic drag coefficients which is necessarily restricted to sphere-tangent ogive-noses is incorporated into the NSWC computer code.<sup>1</sup>

## ANALYSIS

### Implicit Unsteady Euler Equation Method

The partial differential equations governing the two-dimensional planar or axisymmetric flow of an unsteady inviscid, non-heat-conducting, ideal gas are written in conservation-law form under the generalized independent variable transformation

$$\begin{aligned}\tau &= t, \\ \xi &= \xi(t, x, y), \\ \eta &= \eta(t, x, y)\end{aligned}$$

as follows:

$$(U/J)_{\tau} + [(\xi_t U + \xi_x E + \xi_y F)/J]_{\xi} + [\eta_t U + \eta_x E + \eta_y F]/J]_{\eta} + jH = 0 \quad (1)$$

where

$$U = \begin{bmatrix} \rho \\ \rho u \\ \rho v \\ e \end{bmatrix} \quad E = \begin{bmatrix} \rho v \\ p + \rho u^2 \\ \rho uv \\ (e+p)u \end{bmatrix} \quad F = \begin{bmatrix} \rho v \\ \rho uv \\ p + \rho v^2 \\ (e+p)v \end{bmatrix} \quad H = \frac{1}{yJ} \begin{bmatrix} \rho v \\ \rho uv \\ \rho v^2 \\ (e+p)v \end{bmatrix}$$

and the Jacobian

$$J = \xi_x \eta_y - \xi_y \eta_x.$$

In eq. (1),  $j = 0$  for two-dimensional flow;  $j = 1$  for axisymmetric flow (where  $y$  becomes the cylindrical radius);  $p$  represents the pressure,  $\rho$ , the density;  $u$  and  $v$ , the velocity components in the  $x$  and  $y$  directions, respectively; and  $e$ , the total energy per unit volume. The following equation relates the pressure, density, and velocity components to the energy for an ideal gas

$$e = p/(\gamma-1) + \rho(u^2 + v^2)/2 \quad (2)$$

The equations represented by eq. (1) were solved using an implicit Euler equation method.

Using the above independent variable transformation, the physical plane with boundaries 1-4 in  $x$ ,  $y$ , and  $t$  space is mapped into the rectangular computational plane  $\xi$ ,  $\eta$ , and  $\tau$  space as shown in figure 1. The metrics (geometric factors) that are required by eq. (1) are defined as follows:

$$\begin{aligned}\xi_t &= (x_\eta y_\tau - y_\eta x_\tau)/I & \eta_t &= (y_\xi x_\tau - x_\xi y_\tau)/I \\ \xi_x &= y_\eta/I & \eta_x &= -y_\xi/I \\ \xi_y &= -x_\eta/I & \eta_y &= x_\xi/I\end{aligned}\tag{3}$$

where

$$I = 1/J = x_\xi y_\eta - x_\eta y_\xi.$$

Generally at each time step the metrics of eq. (3) are not known analytically and they must be determined numerically.

The basic numerical algorithm used in the IMP code was developed by Beam and Warming.<sup>4</sup> It is second-order accurate, noniterative, and is in a spatially factored form. In particular, the "delta-form" with Euler time differencing is used, and when applied to eq. (1), it assumes the following form

$$(I + \Delta t \delta_\xi A^n)(I + \Delta t \delta_\eta B^n)(U^{n+1} - U^n) = -\Delta t(\delta_\xi E^n + \delta_\eta F^n + H_j)\tag{4}$$

where  $A$  and  $B$  are the Jacobian matrices  $A = \partial \hat{E} / \partial \hat{u}$  and  $B = \partial \hat{F} / \partial \hat{u}$  with  $\hat{u} = U/J$ ;  $\hat{E} = (\xi_t U + \xi_x E + \xi_y F)/J$ , and  $\hat{F} = (\eta_t U + \eta_x E + \eta_y F)/J$ . The  $A$  matrix is given below. The  $B$  matrix, which has the same form except that  $\xi_t$ ,  $\xi_x$ , and  $\xi_y$  are replaced by  $\eta_t$ ,  $\eta_x$ , and  $\eta_y$ , is not presented.  $I$  is the identity matrix,  $\delta_\xi$  and  $\delta_\eta$  are second-order, central difference operators,  $\hat{u}^{n+1} = \hat{u}(n\Delta t)$  and  $\Delta t$  is the integration stepsize.



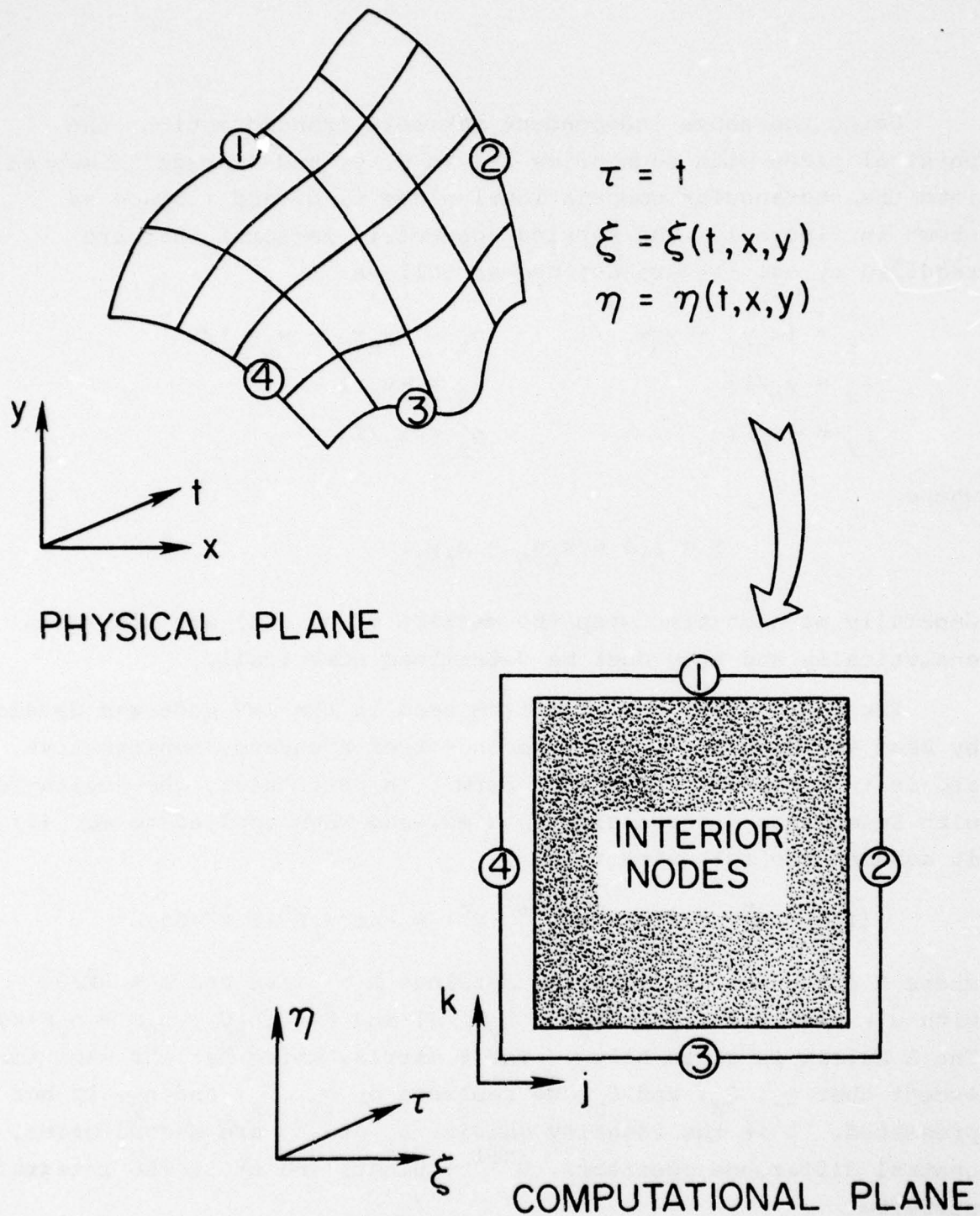


Figure 1. Transformation of Physical Plane to Computational Plane for a Single Solver

$$A = \begin{bmatrix} \xi_t & (\gamma-1)q^2\xi_x/2 & (\gamma-1)q^2\xi_y/2 & [(\gamma-1)q^2-\gamma e/\rho] \cdot \\ & -u(\xi_x u + \xi_y v) & -v(\xi_x u + \xi_y v) & \cdot (\xi_x u + \xi_y v) \\ \xi_x & \xi_t - (\gamma-2)u\xi_x & \xi_x v - \xi_y(\gamma-1)u & [\gamma e/\rho - (\gamma-1)q^2/2]\xi_x - (\gamma-1)u \cdot \\ & + \xi_x u + \xi_y v & & \cdot (u\xi_x + v\xi_y) \\ \xi_y & -\xi_x(\gamma-1)v & \xi_t - (\gamma-2)v\xi_y & [\gamma e/\rho - (\gamma-1)q^2/2]\xi_y - (\gamma-1)v \cdot \\ & + \xi_y u & + \xi_x u + \xi_y v & \cdot (u\xi_x + v\xi_y) \\ 0 & (\gamma-1)\xi_y & (\gamma-1)\xi_y & \xi_t + \gamma(\xi_x u + \xi_y v) \end{bmatrix} \quad (5)$$

Equation (4) is solved at the interior points only. It requires two block  $4 \times 4$ , tridiagonal inversions at each time step of the integration. The solution procedure is as follows:

1. Define  $\Delta \hat{U} = \hat{U}^{n+1} - \hat{U}^n$ ;
2. Form the right-hand side of (4) and store results in the  $\hat{U}^{n+1}$  array;
3. Apply smoothing  $\hat{U}^{n+1} = \hat{U}^{n+1} - \epsilon/8 S/J$  where the smoothing term is defined below;
4. Define  $\bar{U} = (I + \Delta t \delta_\eta B^n) U$  and solve the matrix equation  $(I + \Delta t \delta_\xi A^n) \bar{U} = U^{n+1}$  for  $\bar{U}$  and again store the result in the  $\hat{U}^{n+1}$  array;
5. Solve the matrix equation  $(I + \Delta t \delta_\eta B^n) \Delta \hat{U} = \hat{U}^{n+1}$  for  $\Delta \hat{U}$ ;
6. Obtain the new values of  $\hat{U}^{n+1}$  from the equation  $\hat{U}^{n+1} = \Delta \hat{U} + \hat{U}^n$ .

A fourth order smoothing term is needed to eliminate nonlinear instabilities<sup>3</sup> which arise since the use of central differences in the spatial directions results in a neutrally stable algorithm. The smoothing term  $S$  is

$$\begin{aligned}
 S_{jk} = & (\hat{U}_J)_{j+2,k}^{n+1} - 4[(\hat{U}_J)_{j+1,k}^{n+1} + (\hat{U}_J)_{j-1,k}^{n+1}] + 12(\hat{U}_J)_{j,k}^{n+1} \\
 & + (\hat{U}_J)_{j-2,k}^{n+1} + (\hat{U}_J)_{j,k+2}^{n+1} - 4[(\hat{U}_J)_{j,k+1}^{n+1} + (\hat{U}_J)_{j,k-1}^{n+1}] \\
 & + (\hat{U}_J)_{j,k-2}^{n+1}
 \end{aligned} \tag{6}$$

and  $\xi$  is the smoothing coefficient chosen from the range  $0 \leq \xi \leq 0.4$  depending upon the size of the time step. The  $j$  and  $k$  indices correspond to the  $\xi$  and  $\eta$  directions, respectively. At the points adjacent to the boundaries a special form of the smoothing term is used.

The solution of initial value problems using finite difference procedures requires an integration step size. The value of this step size is a function of the eigenvalues of the coefficient matrices,  $\bar{A}$  and  $\bar{B}$ , of the governing pde's (equation 1) when written in the form:

$$u_\tau + \bar{A}u_\xi + \bar{B}u_\eta + j\hat{H} = 0 \tag{7a}$$

The eigenvalues of the coefficient matrices  $\bar{A}$  and  $\bar{B}$  are

$$\begin{aligned}
 \sigma_{A_{1,2}} &= \xi_t + u\xi_x + v\xi_y \pm c(\xi_x^2 + \xi_y^2)^{1/2} \\
 \sigma_{A_3} &= \xi_t + u\xi_x + v\xi_y \\
 \sigma_{B_{1,2}} &= \eta_t + u\eta_x + v\eta_y \pm c(\eta_x^2 + \eta_y^2)^{1/2} \\
 \sigma_{B_3} &= \eta_t + u\eta_x + v\eta_y
 \end{aligned} \tag{7b}$$

where  $\hat{H}$  is the modified source term and



where  $c$ , the speed of sound is equal to  $(\gamma p/\rho)^{1/2}$ . The  $\sigma$  terms in Eq. (7b) can be recognized as the slopes of the characteristics and streamlines in the  $t$ - $\xi$  and  $t$ - $\eta$  planes.

The stability theory for explicit methods, at least for  $(t, \xi)$  space in unsteady flow, requires that

$$\frac{\Delta t}{\Delta \xi} \leq \frac{1}{|(\sigma_{A_\ell})_{\max}|} \quad \ell = 1, 3 \quad (8b)$$

where  $(\sigma_{A_\ell})_{\max}$  is the maxima of the local eigenvalues of all the points at a particular constant  $t$  or  $\xi$  plane. Similar relations can be obtained for the  $(t, \eta)$  plane:

$$\frac{\Delta t}{\Delta \eta} \leq \frac{1}{|(\sigma_{B_\ell})_{\max}|} \quad \ell = 1, 3 \quad (8c)$$

This planar analysis has been shown to give a good bound on the step size in multidimensional problems if the right hand side of Eqs.

(8b) and (8c) are multiplied by a constant  $C$ . In explicit methods,  $C \leq 1$  and is usually assigned a value of 0.9 whereas in implicit methods  $C$  is only restricted by the accuracy of the solution since implicit methods are unconditionally stable. Typically these values are on the order of 5 to 10 for inviscid flow computations.

It is convenient to consider two types of boundaries in inviscid computational fluid dynamics - those which are impermeable (no mass flow across) and those which are permeable (mass flow across). The impermeable boundaries consist of such surfaces as solid walls, symmetry planes and slip surfaces, while the permeable boundaries consist of such things as supersonic inflow or outflow boundaries and shock waves. In the transonic flow about projectiles, the four boundaries of figure 1 can be characterized as follows: boundary 1 is either a shock wave ( $M_\infty > 1.00$ ) or a fixed outer boundary ( $M_\infty < 1.0$ ), boundary 2 is an outflow plane, boundary 3 is the solid body, and boundary 4 the plane of symmetry.

The body boundary is treated by using the tangency condition which is incorporated through the use of Kentzer's scheme,<sup>6</sup> and at the symmetry plane, the variables are reflected according to whether they are odd or even. The outflow boundary is placed far enough down the aft body such that the pressure can be approximated by its value at infinity and the rest of the variables are extrapolated. At the outer boundary, there are two possibilities: (1) if shock fitting is used and the flow is supersonic, the sharp discontinuity approach of Thomas<sup>7</sup> is used or (2) if shock capturing is used, the flow can be either subsonic or low supersonic and the outer boundary is chosen such that its influence on the flow field surrounding the body is negligible.

The initial conditions are determined by first guessing a shock wave shape or outer boundary shape for the particular obstacle at hand. Second, a Newtonian pressure distribution is prescribed on the body. Using the fact that there is no flow through the body and that the maximum entropy streamline wets the body, the remainder of the properties can be prescribed on the body. Finally, a linear variation for the properties is prescribed between boundary 1 and the body. This gives an initial guess for the flow field which is integrated forward in time until a steady state is reached.

In all cases, the resulting flow field between the body and the outermost boundary is treated in shock capturing fashion and, therefore, allows for the correct formation of secondary internal shocks.

Applying the algorithm, boundary conditions and initial conditions to Eq. (1) and solving Eq. (1) in a time asymptotic fashion with interest only in the steady state, a complete set of flow field data results out of which the nose drag is calculated by integrating the surface pressures over the surface area of the body.

#### Drag Calculation

The wave or pressure drag for a sphere-ogive-cylinder body at zero angle of attack is

$$D = \int_0^{2\pi} \int_0^{y_b} (p - p_\infty) y \, dy \, d\phi \quad (9)$$

(see figure 2). Note that  $p - p_\infty$  is the differential pressure along the surface and  $y d\phi \cdot dy$  is the surface area over which the pressure is acting for drag considerations. Since the body is axisymmetric and at zero angle of attack, the pressure is not a function of the meridional angle,  $\phi$ . Integrating the above equation (9) and using the fact that  $p - p_\infty = f(y)$  gives

$$D = 2\pi \int_0^{y_b} (p - p_\infty) y \, dy \quad (10a)$$

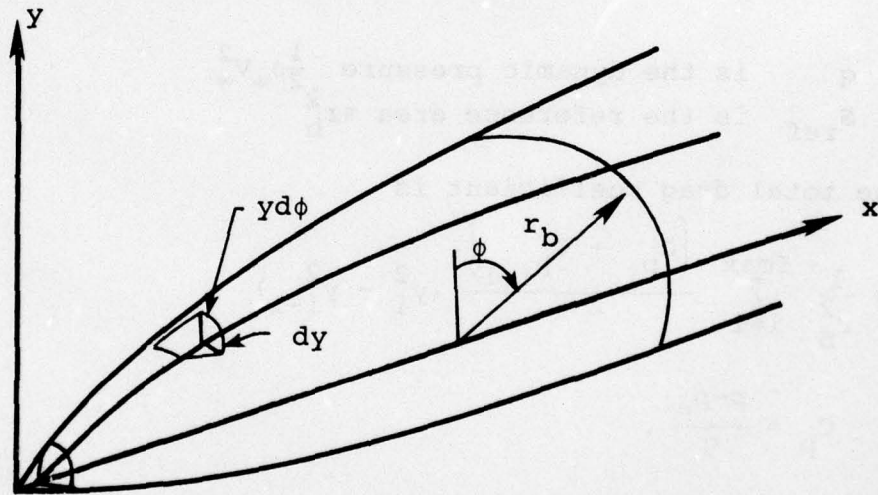


Figure 2. Nomenclature for Drag Calculation

By using the following approximation for total drag

$$D \approx \sum_{i=0}^I D_i \quad (10b)$$



equation (10) can be integrated using the mean value theorem for each geometric segment  $i$ . This can be written as a form of the trapezoidal rule

$$D \approx 2\pi \sum_{i=1}^I (\overline{p-p_\infty}) \frac{(y_i^2 - y_{i-1}^2)}{2} \quad (10c)$$

where

$$(\overline{p-p_\infty}) = \frac{(p-p_\infty)_i + (p-p_\infty)_{i-1}}{2}$$

Thus the total drag is the summation of each geometric increment of drag.

The drag coefficient is defined as

$$C_D = \frac{D}{qS_{\text{ref}}} \quad (11a)$$

where

$$\begin{aligned} q & \text{ is the dynamic pressure } \frac{1}{2}\rho_\infty V_\infty^2 \\ S_{\text{ref}} & \text{ is the reference area } \pi r_b^2 \end{aligned}$$

Finally, the total drag coefficient is

$$C_D = \frac{1}{r_b^2} \sum_{i=1}^{I_{\text{max}}} \frac{(C_{p_i} + C_{p_{i-1}})}{2} (y_i^2 - y_{i-1}^2) \quad (11b)$$

where

$$C_p = \frac{p-p_\infty}{q}$$

### Body Geometry

A large number of ogive body shapes are considered in this report. They are characterized by bluntness ratios from 0 to 1 and fineness ratios from 5 to 0.5.

From figure 3, the bluntness ratio is defined as the nose radius divided by the cylindrical body radius

$$\text{Bluntness} = \frac{R_n}{R_b}$$

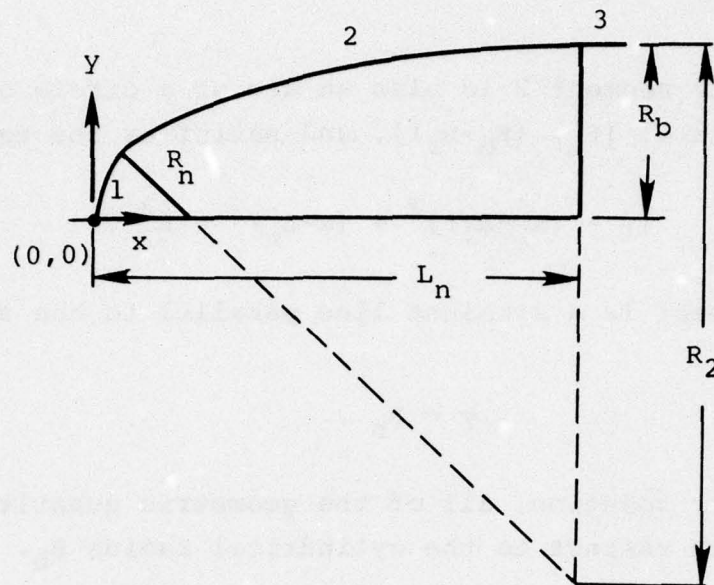


Figure 3. Ogive body geometry definition

where a bluntness of 0 is a pointed ogive and a bluntness of 1 is a hemisphere. The fineness ratio is defined as the sphere ogive body length divided by the diameter of the attached cylinder:

$$\text{Fineness} = \frac{L_n}{2R_b}$$

where a fineness ratio of 0.5 is a hemisphere cylinder.

Geometrically, the sphere ogive cylinder configuration is defined by using one algebraic equation in  $y$  and  $x$  to define each of the three segments which are shown in figure 3. This general equation is written

$$Ay^2 + Byx + Cx^2 + Dy + Ex + F = 0$$

where the coefficients vary depending upon which segment of the body is being defined. Body segment 1 is input as the arc of a circle of radius  $R_n$  with the origin at  $(R_n, 0)$  and it satisfies the equation

$$y^2 + (x - R_n)^2 = R_n^2$$

Similarly, body segment 2 is also an arc of a circle of radius  $R_2$  with the origin at  $[L_n, (R_b - R_2)]$ , and satisfies the equation

$$[y - (R_b - R_2)]^2 + (x - L_n)^2 = R_2^2 .$$

The third segment is a straight line parallel to the x axis and is given by

$$y = R_b .$$

In the computer solution, all of the geometric quantities are normalized with respect to the cylindrical radius  $R_b$ .

#### Table Lookup Method

The wave or pressure drag coefficient has been calculated as a function of three variables,

$$C_D = f(M_\infty, R_n/R_b, L_n/R_b) .$$

The problem is one of interpolation for the drag coefficient given the three independent variables. This can be done by three one-dimensional interpolations. To keep within the framework of the previous program usage and for the ease of understanding, the following approach was taken. In this process, the table of drag coefficients consists of 10 nose bluntnesses, 8 nose lengths, and 4 Mach numbers. The procedure is as follows:

1. For a single value of bluntness, load up a new set of 8 nose length arrays each consisting of drag values for the four corresponding Mach numbers; i.e.  $L_i = L_i(C_D(M_\infty))$   
 $i = 1, 2, \dots, 8.$



2. For a given Mach number, a three point Lagrangian interpolation is used to obtain a value of the drag coefficient from each of the 8 new nose length arrays of step 1. Each interpolated value is stored in a new array corresponding to one of the 8 nose lengths.
3. For a given nose length, a five point Lagrangian interpolation is used on the new arrays created in step 2 to find the final value of drag which is stored in a new array.
4. Steps 1 through 3 yield the drag coefficient for a single value of bluntness in the drag table and for the given Mach number and nose length. Repeating steps 1 through 3 for each value of nose bluntness, a value for the drag coefficient is obtained for each bluntness.
5. A five point Lagrangian interpolation is performed on the drag coefficient array of step 3 which consists of a value for each of the 10 bluntness in the table. This gives the final value of the drag coefficient for a specified Mach number, nose length, and nose bluntness.

Two subroutines not available in the NSWC parent code were needed in this solution procedure. They are documented in a later section.

## RESULTS AND DISCUSSION

### Comparison of Pressure Prediction Methods

Since there is experimental data<sup>8</sup> readily available through the transonic range for hemisphere cylinders, the present technique was initially applied to that limiting case. These results are presented in figures 4-10.

Figure 4 shows the typical grid network used. By numerical experimentation, it was found that locating the outer boundary at 10 body diameters and the outflow boundary at 4 body diameters was sufficient to obtain a solution uninfluenced by the choice of boundaries. It was also found useful to stretch the mesh in the outer regions and compress it near the body.

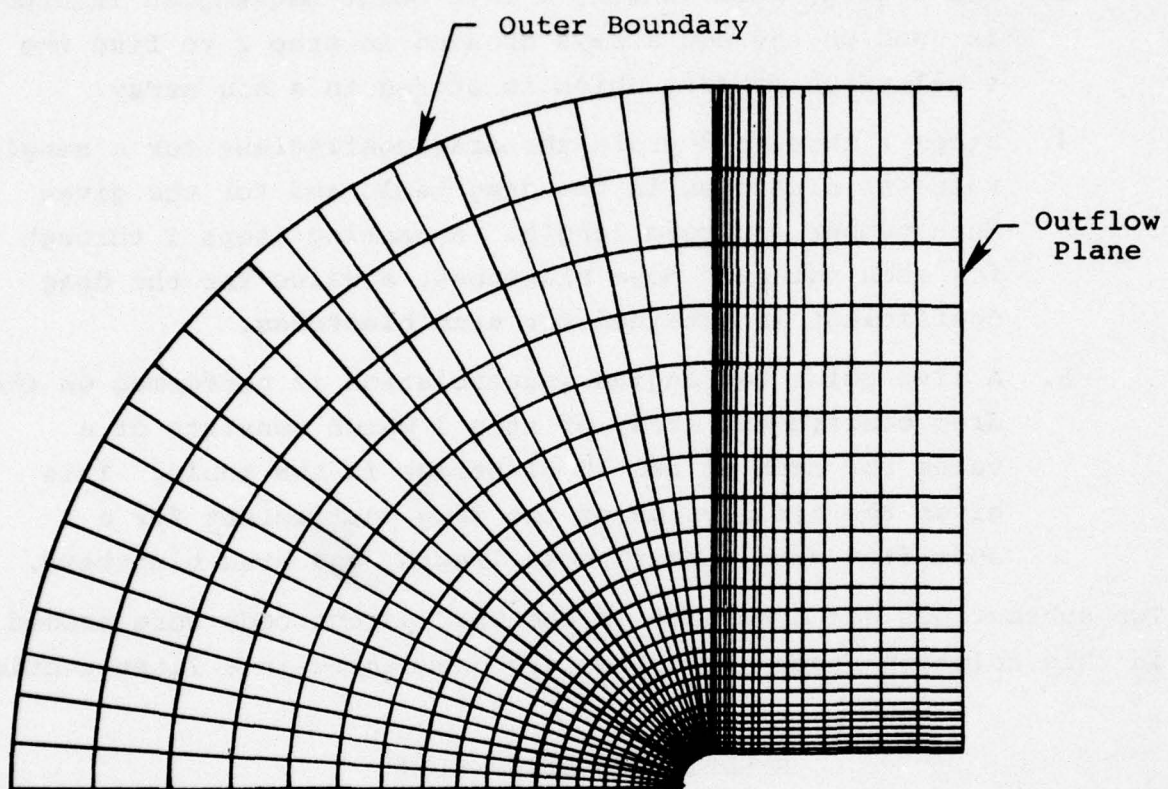


Figure 4. Typical Example of Computational Grid



Figure 5 shows numerical results from the present method compared to the experiments performed by Hsieh for  $M_\infty = .7, .95, 1.0, 1.05, 1.1$ . In all cases, the comparison is very good with experiment. This establishes confidence in the present method.

Figure 6 compares numerical computations of the drag for a hemisphere-cylinder with Hsieh's experimental results. The drag calculation by the present method gives good agreement with the previous numerical and experimental results of Hsieh.<sup>8</sup>

The flow field of a highly supersonic flow is presented in figure 7. The typical transonic flow pattern is observed with an acceleration of flow over the hemisphere nose to sonic velocity and downstream compression on the cylinder via a normal shock wave.

Figures 8 and 9 show, respectively, the shock angle which is measured from the horizontal,  $\delta$ , and the shock wave and sonic line for low supersonic flow,  $M_\infty = 1.1$  flow over a hemisphere-cylinder. In figure 9, one of the more interesting features of the flow field is the bending back of the sonic line past the vertical axis.

Figure 10 shows the drag (pressure) evolution for transonic flows over a hemisphere-cylinder. Note that in general the limiting value for drag is reached by the time 1200 iterations have been performed.

The results presented above have established the accuracy and versatility of the present code. The next step is to apply it to transonic flow over sphere-ogive-cylinders. Previous researchers<sup>2</sup> have used an inviscid transonic approximation theory to calculate the entire flow field around nonlifting slender ogive bodies. The transonic flow fields are essentially the same for these shapes which include the hemisphere cylinders as a special case. Figures 11 and 12 give some results for different sphere-ogive-cylinder bodies. The calculated pressure distribution along the body for  $M_\infty = 0.95$ , 4 caliber tangent ogive body is presented in figure 11 along with available experimental data. The final mesh point distribution used in calculating the pressure distribution was used in the remaining calculations based on its ability to capture the essentials of a flow field surrounding sphere-ogive-cylinders.



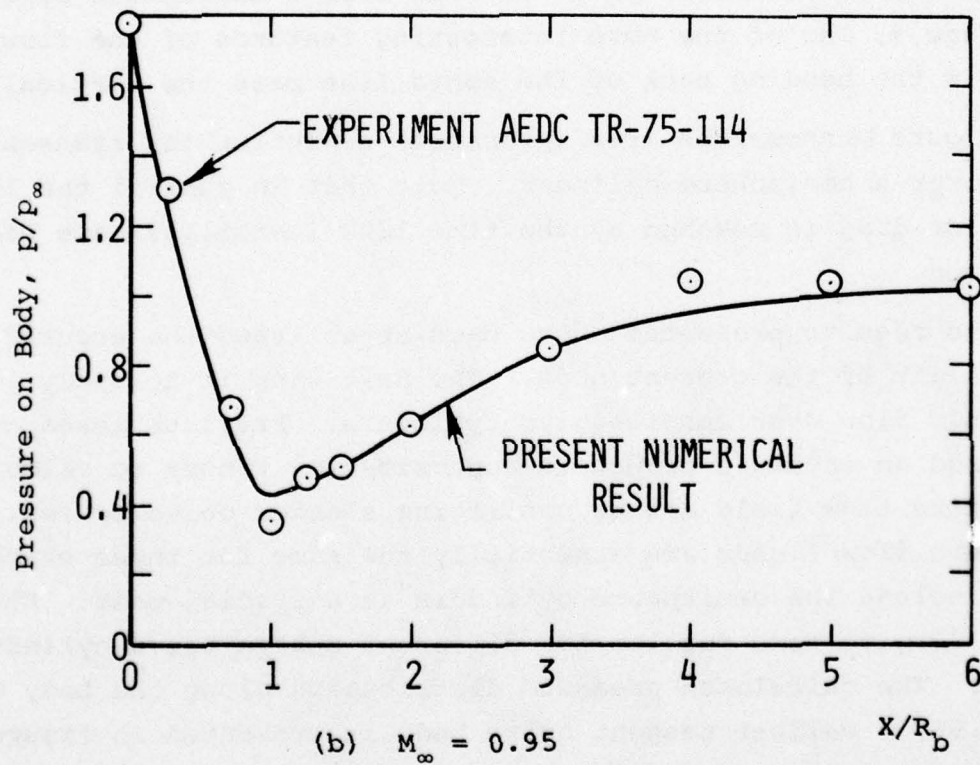
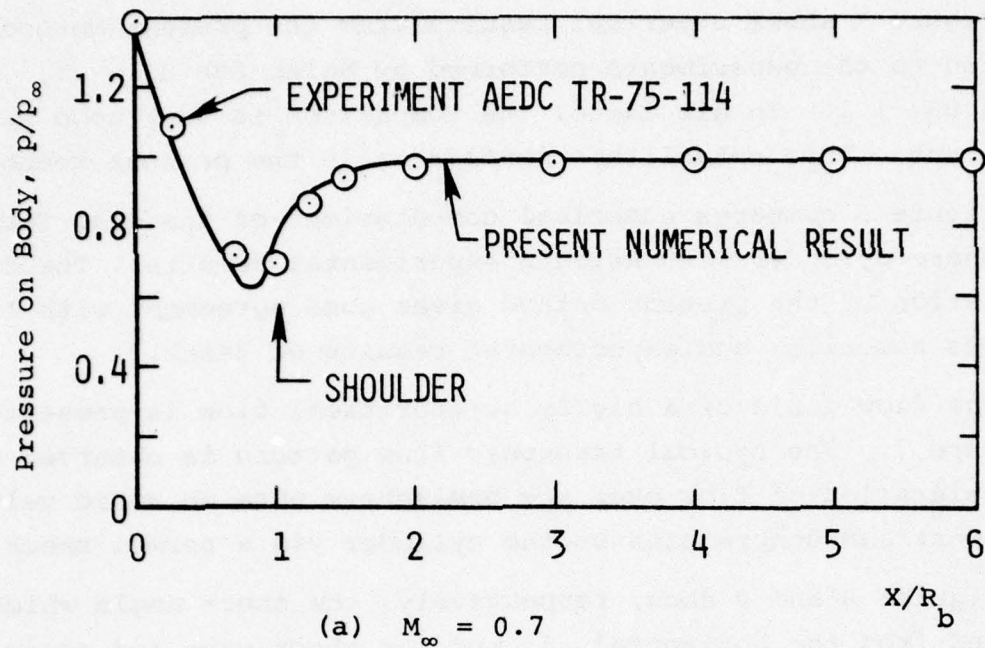


Figure 5. Pressure Distribution on Hemisphere-Cylinder

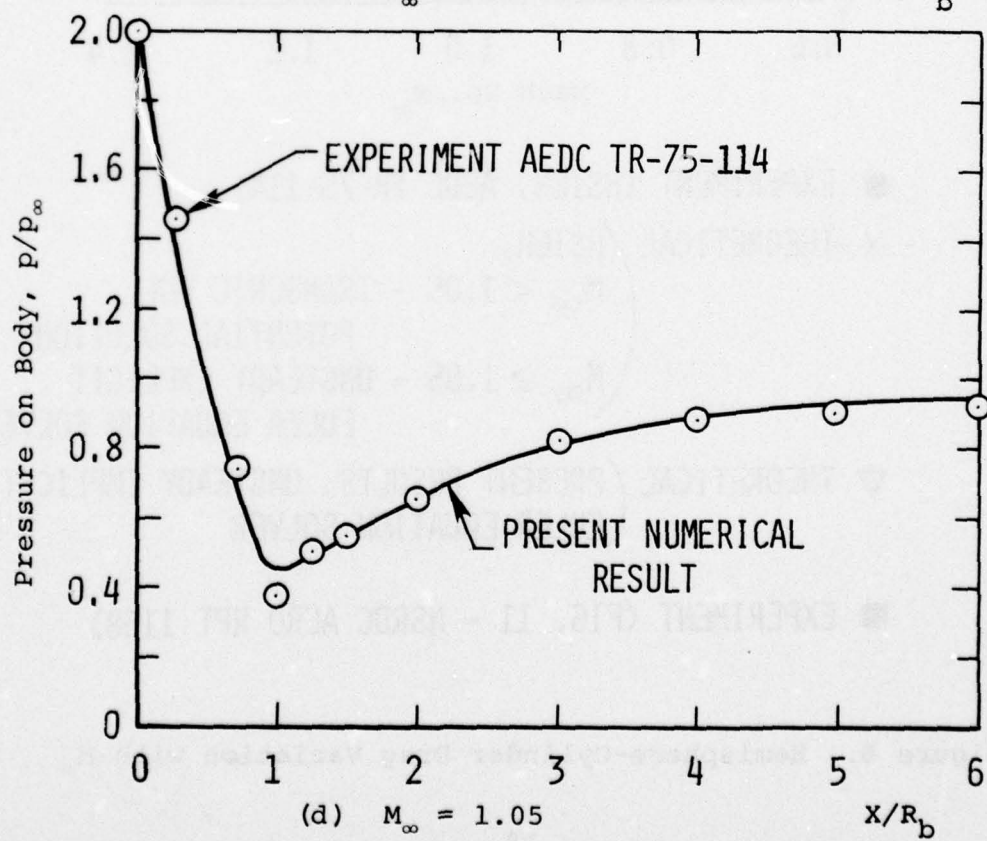
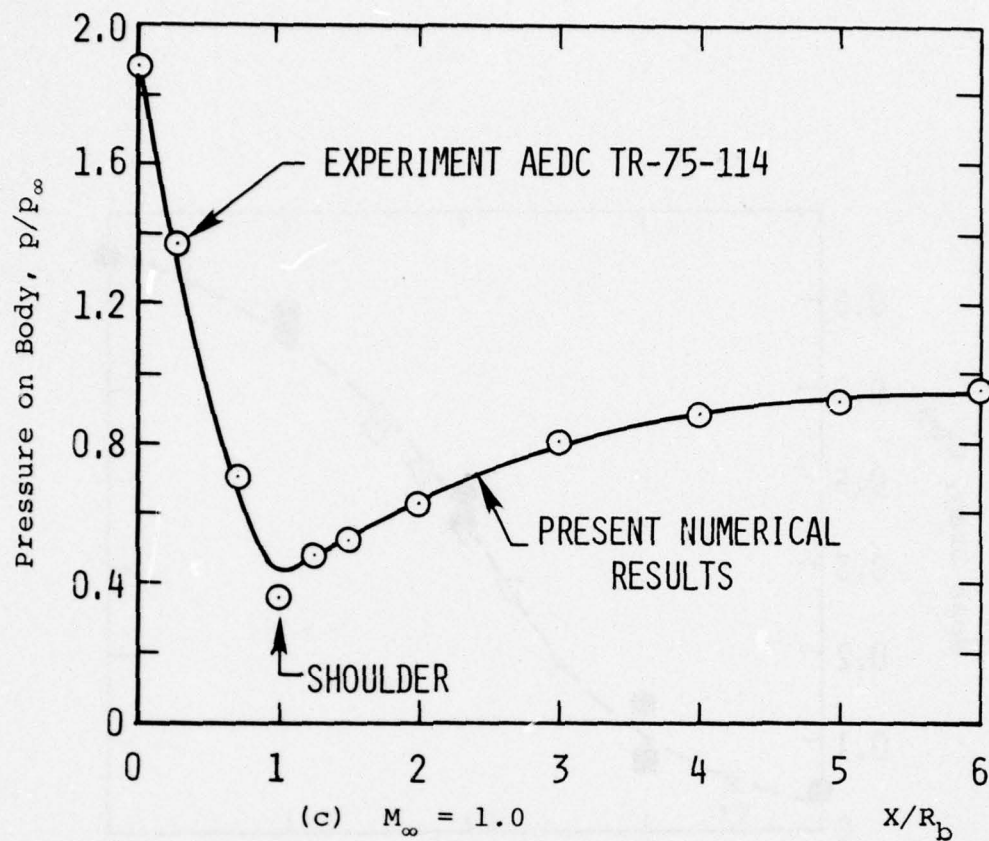
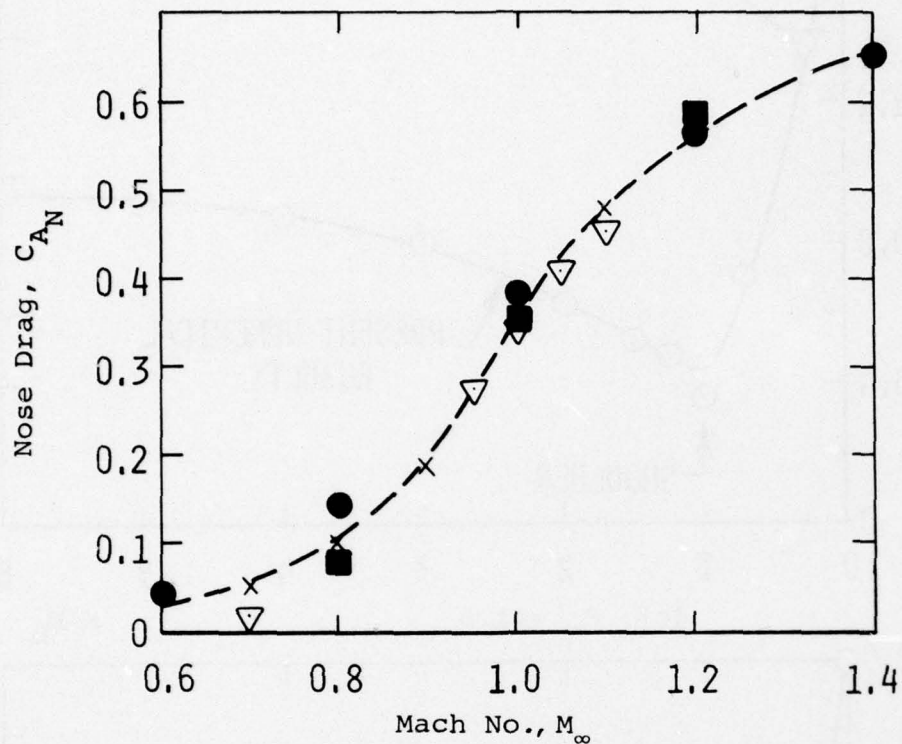


Figure 5. Concluded



- EXPERIMENT (HSIEH, AEDC TR-75-114)
- X--THEORETICAL (HSIEH,
  - $M_{\infty} < 1.05$  - TRANSONIC FULL POTENTIAL SOLUTION
  - $M_{\infty} \geq 1.05$  - UNSTEADY EXPLICIT EULER EQUATION SOLVER
- ▽ THEORETICAL (PRESENT RESULTS, UNSTEADY IMPLICIT EULER EQUATION SOLVER)
- EXPERIMENT (FIG. 11 - NSRDC AERO RPT 1168)

Figure 6. Hemisphere-Cylinder Drag Variation with  $M_{\infty}$



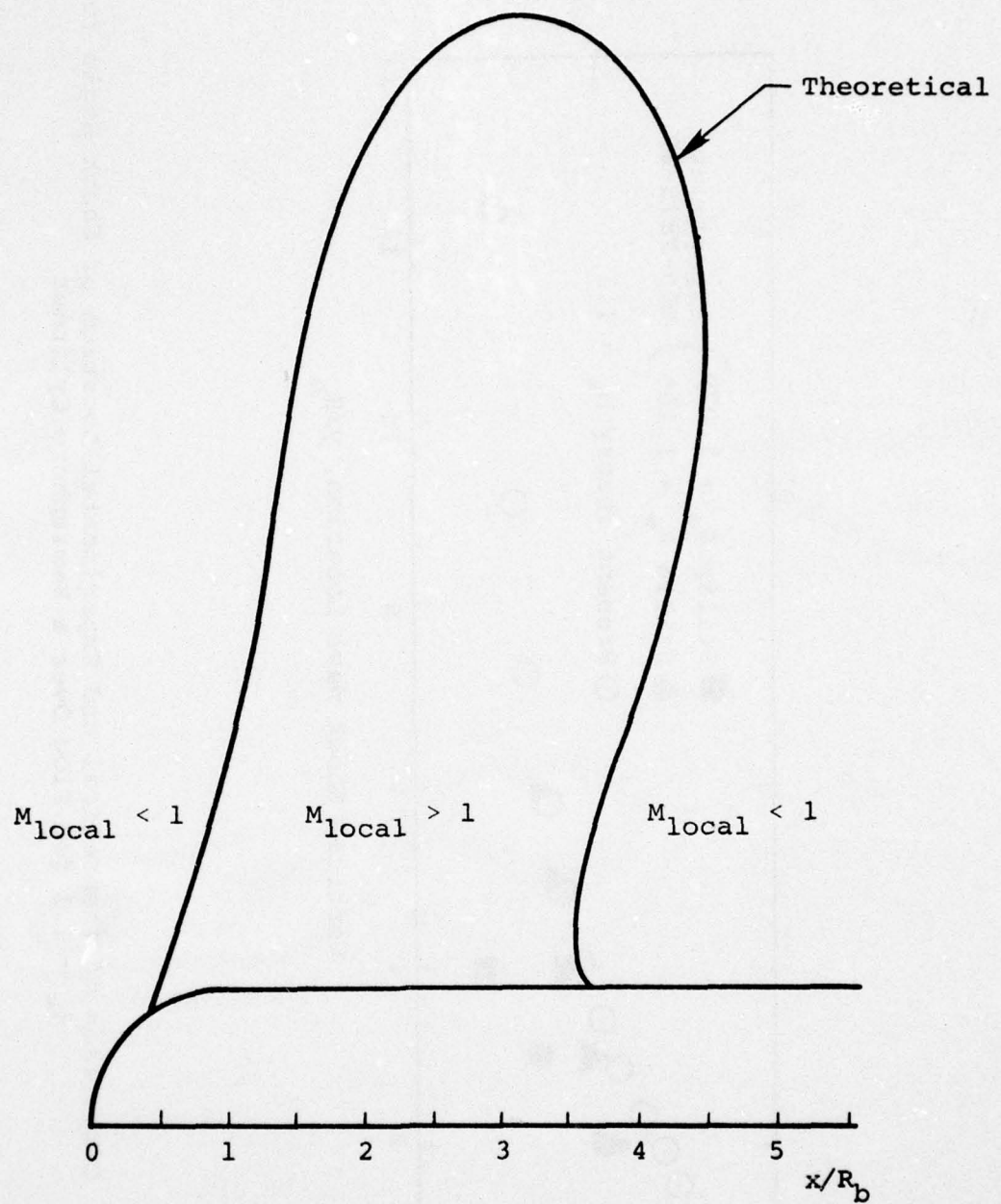


Figure 7. Embedded Supersonic Region at  $M_{\infty} = 0.95$  for Flow Over a Hemisphere Cylinder

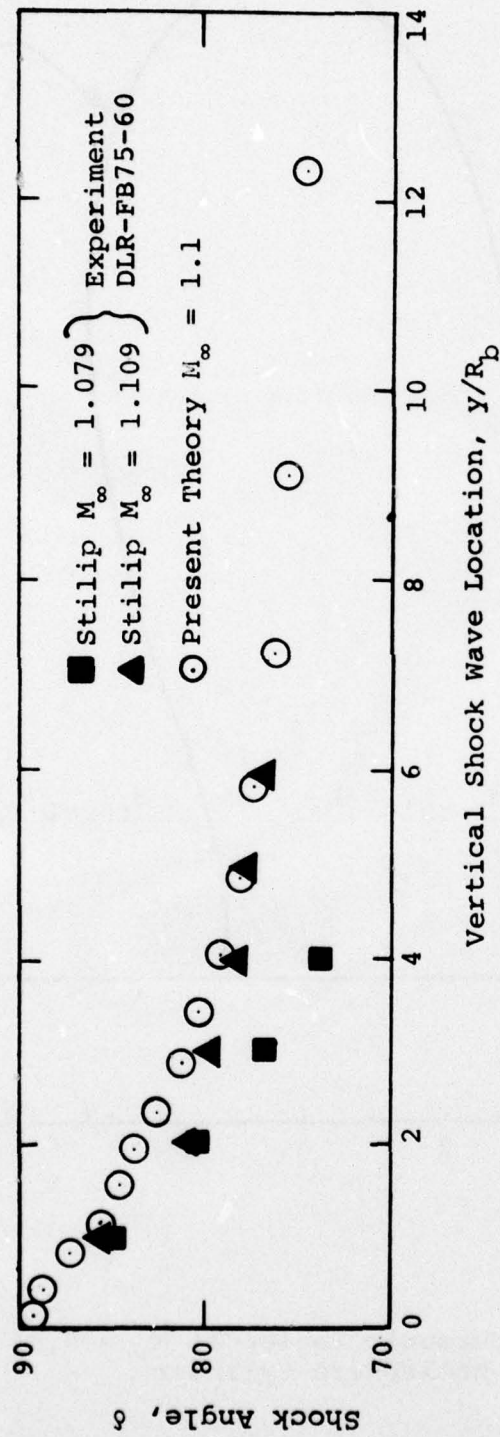


Figure 8. Comparison of Theoretical and Experimental Location of Shock Angle for  $M_\infty = 1.1$  for Flow Over a Hemisphere Cylinder

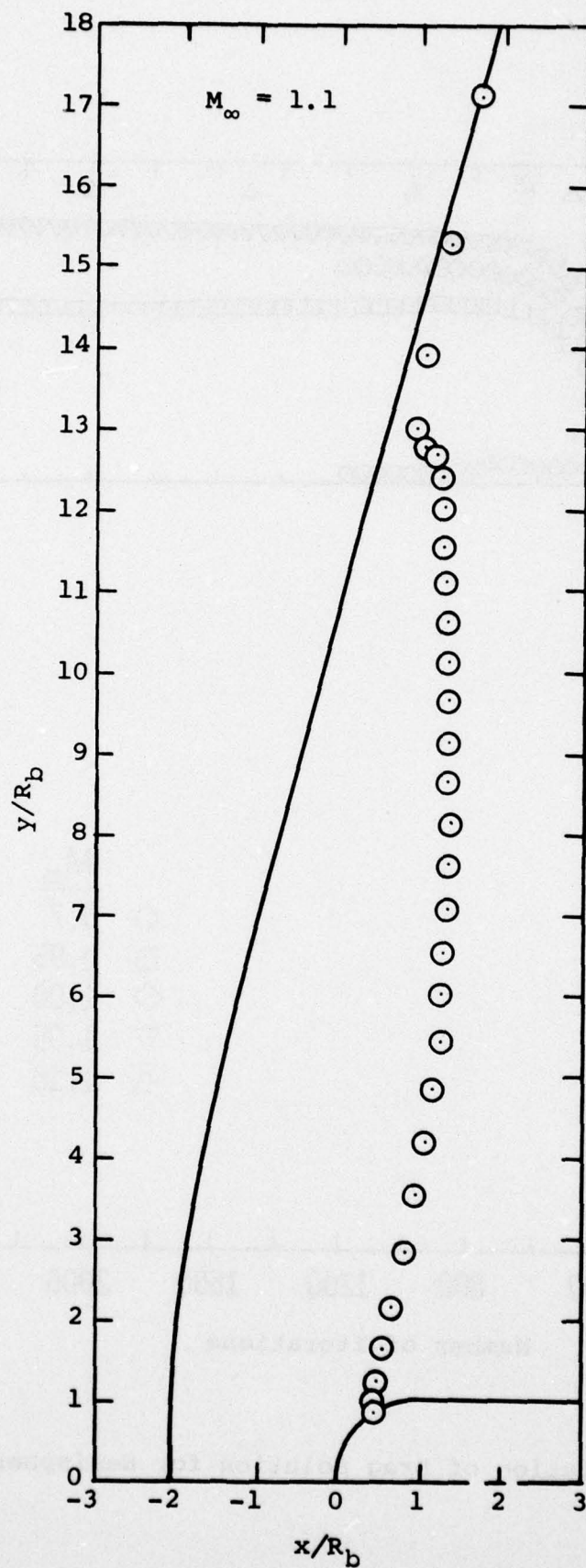


Figure 9. Shock Wave and Sonic Line Location for  $M_\infty = 1.1$  Flow Over a Hemisphere Cylinder



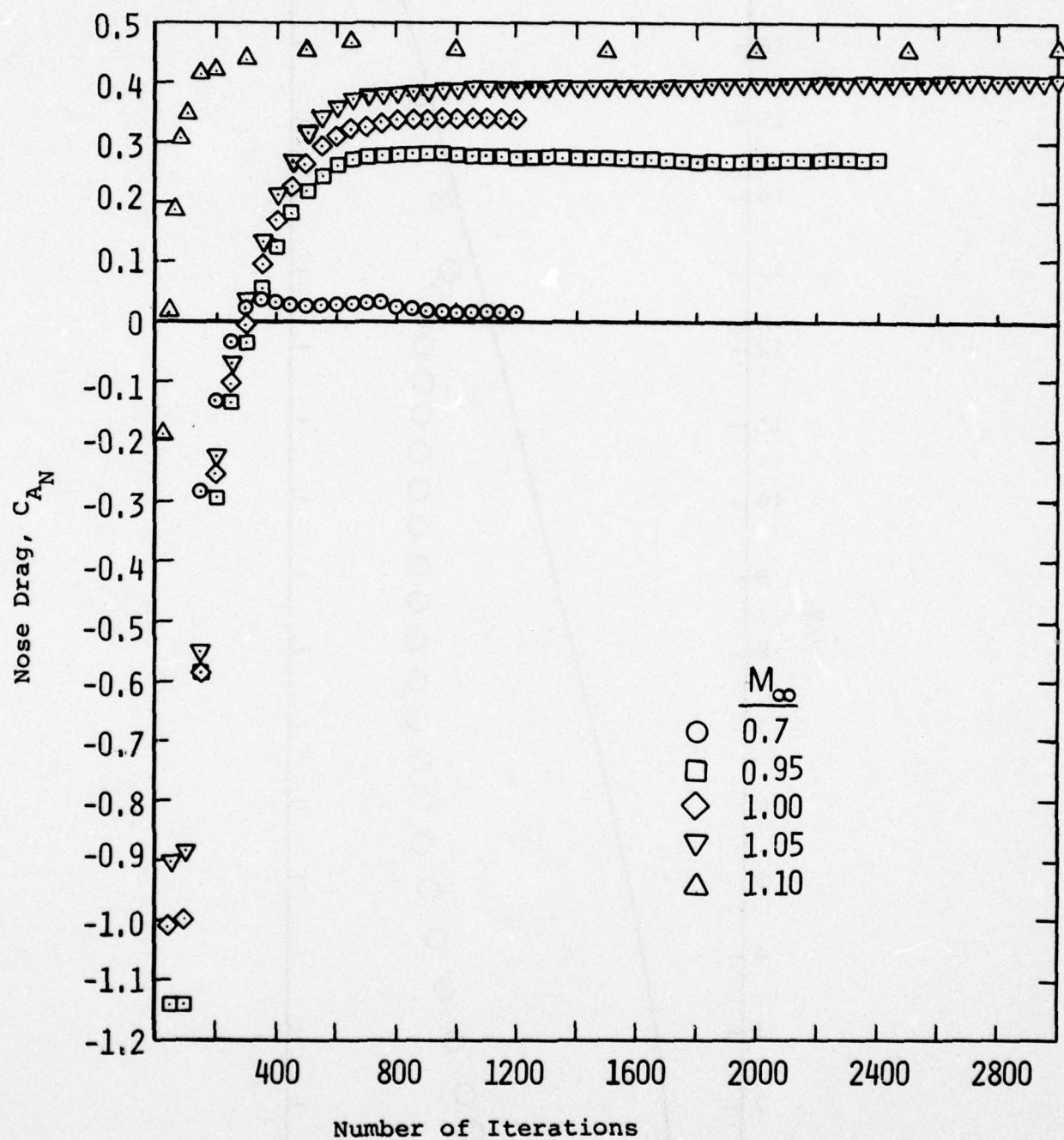


Figure 10. Evolution of Drag Solution for Hemisphere Cylinder

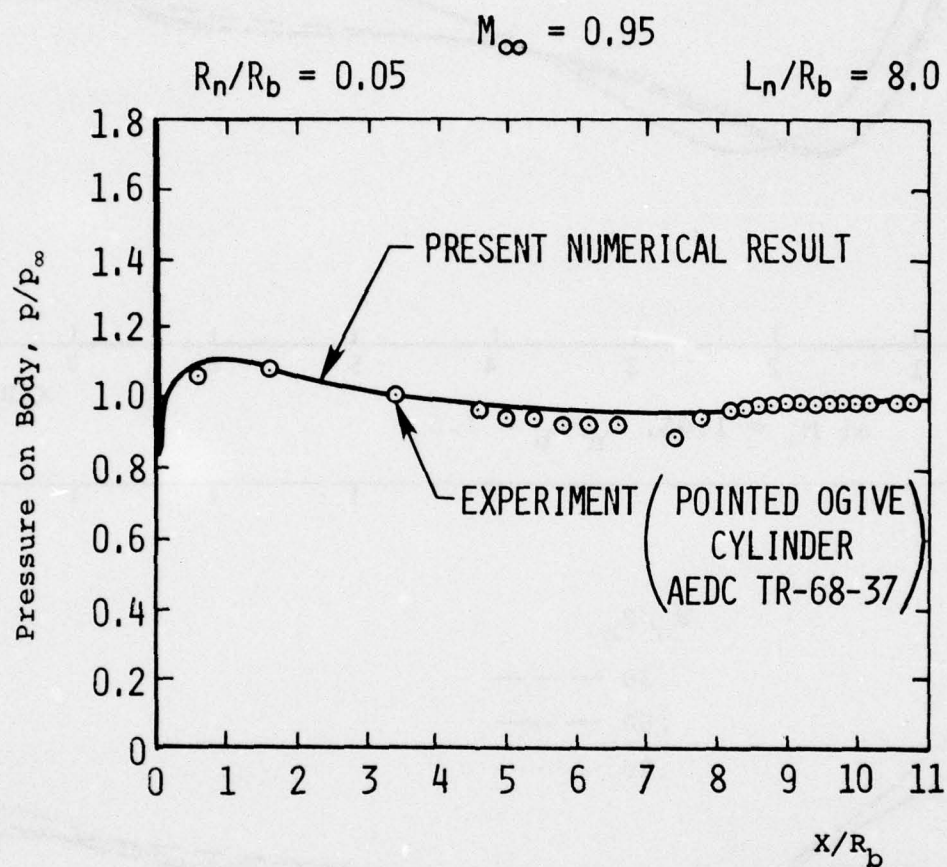


Figure 11. Comparison Between Experiment and Theory for  $M_\infty = 0.95$  Flow Past a 4 Caliber Tangent Ogive Body

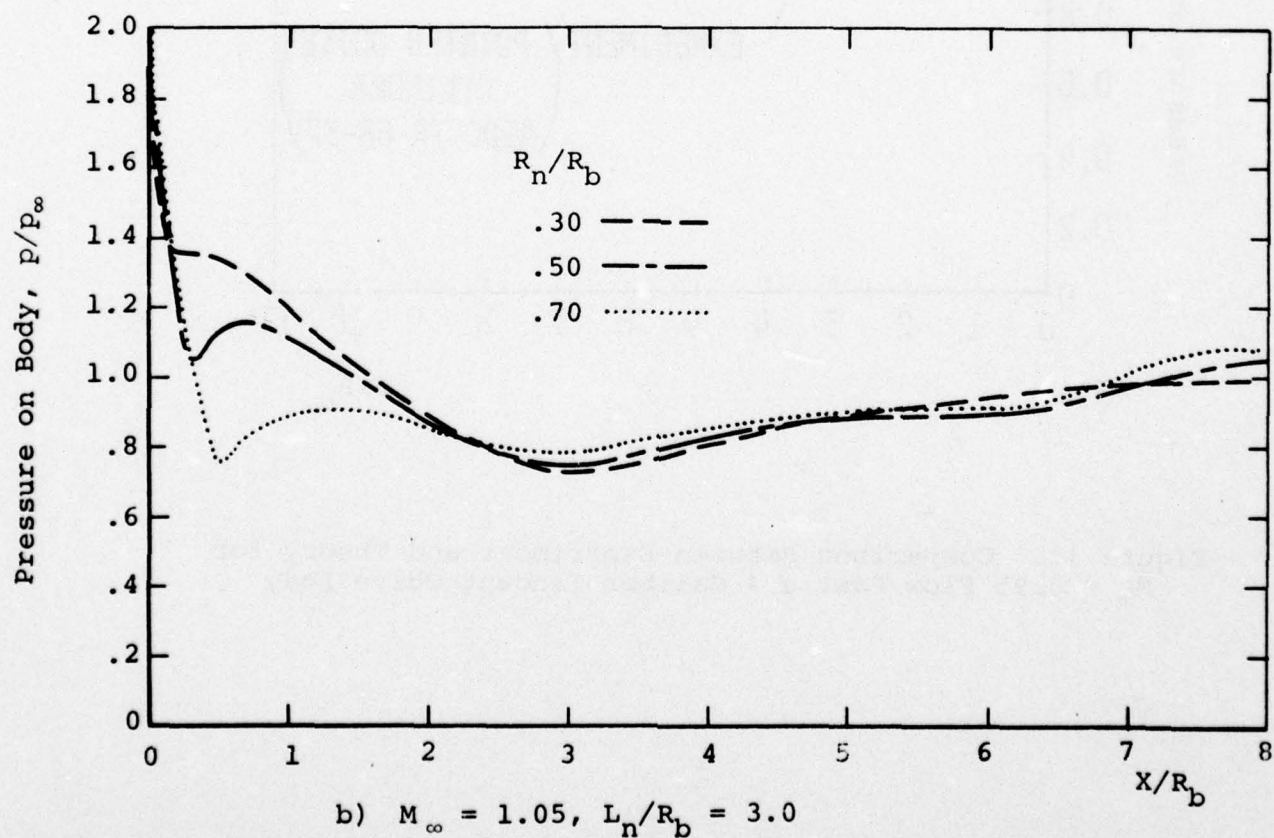
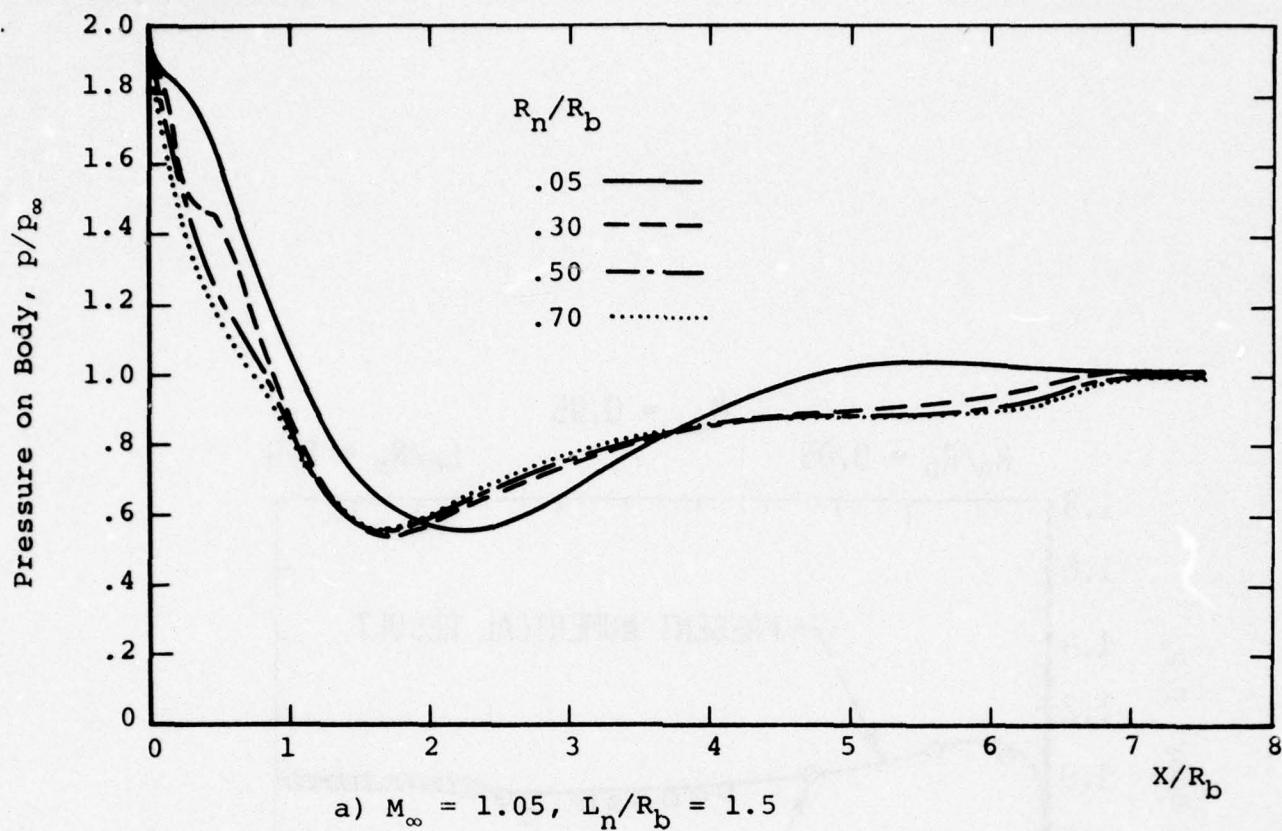
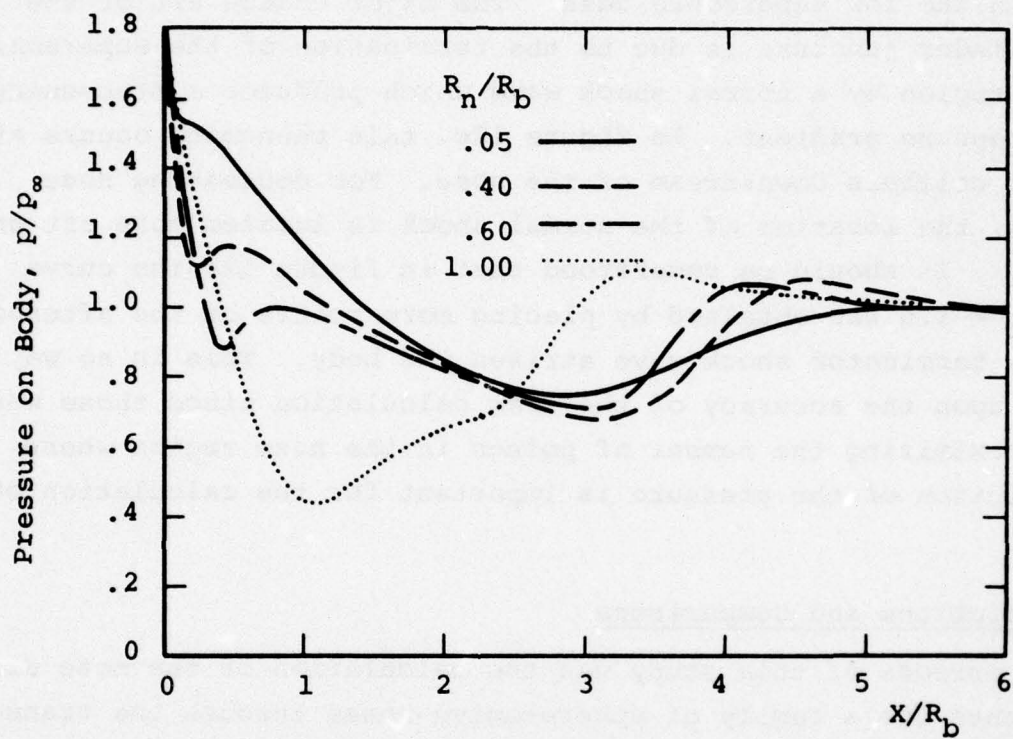


Figure 12. Calculated Body Pressure on Sphere-Ogive-Cylinders for Varying Nose Bluntnesses, Nose Lengths and Mach Numbers





c)  $M_\infty = 0.95$ ,  $L_n/R_b = 3.0$

Figure 12. Concluded

Typical results for transonic flow about sphere-ogive-cylinders are presented in figure 12. Figures 12a and 12b show the effect of nose bluntness and nose length on the body pressure distribution for a  $M_\infty = 1.05$ . The major change in the low supersonic flow regime takes place near the nose of the vehicle. In figure 12c at a high subsonic Mach number,  $M_\infty = 0.95$ , there occurs two major changes, one aft of the ogive-cylinder juncture and one in the region of the nose as in the low supersonic case. The major change aft of the ogive-cylinder juncture is due to the termination of the supersonic embedded region by a normal shock wave which produces a steepening of the pressure gradient. In figure 12c, this phenomena occurs at about 1.5 calibers downstream of the nose. For decreasing nose bluntness, the location of the normal shock is located more aft on the body. It should be understood that in figure 12c the curve for  $R_n/R_b = 1.0$  was obtained by placing more points on the afterbody where the terminator shock wave strikes the body. This in no way reflects upon the accuracy of the drag calculation since those were done by maximizing the number of points in the nose region where the resolution of the pressure is important for the calculation of drag.

#### Drag Predictions and Comparisons

The purpose of this study was the calculation of the nose drag coefficients for a family of sphere-ogive-noses through the transonic Mach number range. A table was constructed (Table I) for these coefficients as a function of nose bluntness, nose length, and Mach number. This table was incorporated into the NSWC computer code. As a first step in obtaining the aforementioned table, nose drag coefficients are presented in figures 13 as a function of nose bluntness and nose length for the transonic Mach numbers 0.8, 0.95, 1.05, and 1.2. To reduce the overall computation time of this study, a minimum matrix of variables was necessarily calculated. These computations are represented by the symbols in figures 13.

In figures 13a, c, e, g, the nose drag coefficient versus nose length with nose bluntness as a variable is presented. For all bluntnesses and for all Mach numbers, the nose drag coefficient

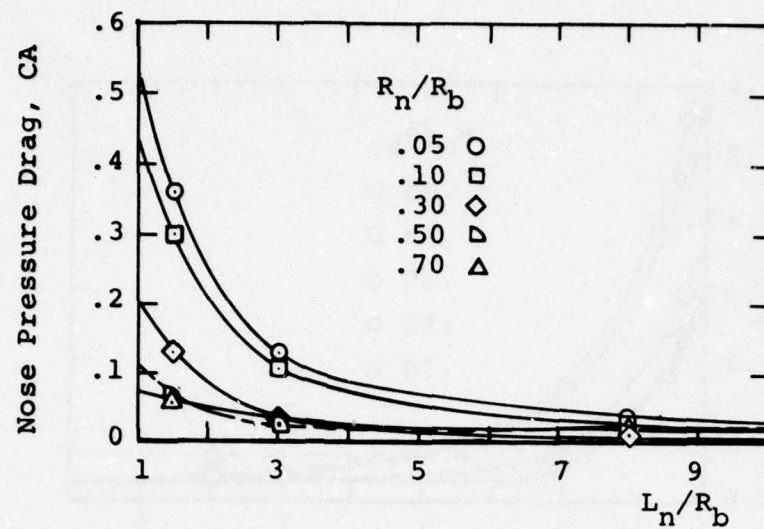


TABLE I.  $C_D = f(R_n/R_b, L_n/R_b, M_\infty)$  for Sphere-Ogive-Cylinders.

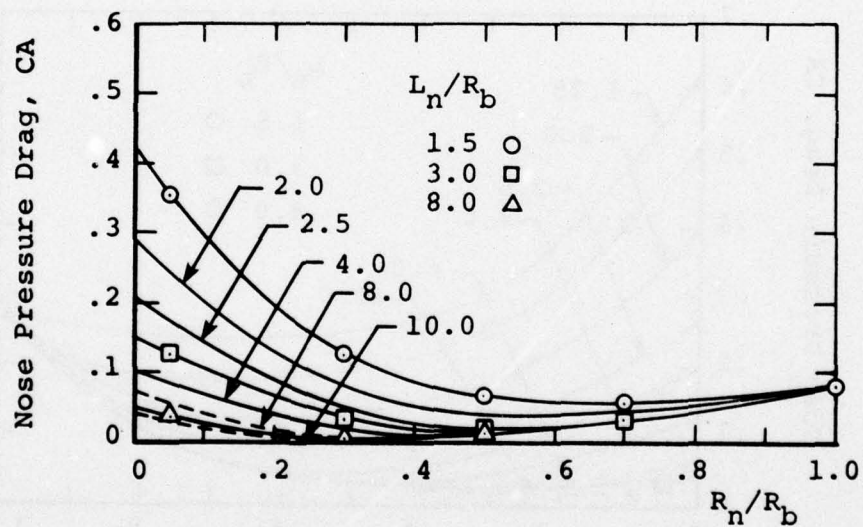
$R_n/R_b$	.0	.1	.2	.3	.4	.5	.6	.7	.8	1.0
$L_n/R_b$										
		$M_\infty = .8$								
1.5	.422	.290	.198	.130	.089	.065	.060	.058	.060	.08
2.0	.290	.200	.130	.081	.051	.040	.040	.045	.055	.08
2.5	.210	.140	.088	.051	.030	.020	.022	.031	.042	.08
3.0	.151	.101	.065	.035	.020	.018	.022	.031	.042	.08
4.0	.100	.070	.040	.020	.010	.010	.020	.031	.042	.08
6.0	.068	.041	.020	.007	.006	.010	.020	.031	.042	.08
8.0	.050	.029	.012	.007	.006	.010	.020	.031	.042	.08
10.0	.041	.020	.008	.007	.006	.010	.020	.031	.042	.08
		$M_\infty = .95$								
1.5	.518	.400	.311	.250	.211	.190	.180	.180	.184	.278
2.0	.395	.295	.223	.175	.144	.130	.123	.238	.150	.278
2.5	.262	.200	.150	.115	.091	.080	.081	.091	.121	.278
3.0	.198	.150	.110	.075	.055	.047	.048	.065	.108	.278
4.0	.130	.091	.061	.042	.040	.031	.048	.065	.108	.278
6.0	.080	.049	.038	.032	.031	.031	.048	.065	.108	.278
8.0	.040	.031	.021	.028	.028	.031	.048	.065	.108	.278
10.0	.025	.020	.015	.020	.021	.031	.048	.065	.108	.278
		$M_\infty = 1.05$								
1.5	.67	.541	.441	.365	.335	.310	.291	.285	.300	.410
2.0	.505	.409	.339	.290	.260	.240	.229	.223	.240	.410
2.5	.390	.321	.270	.230	.202	.180	.170	.170	.200	.410
3.0	.302	.250	.210	.180	.160	.145	.135	.130	.175	.410
4.0	.211	.175	.140	.115	.100	.095	.100	.121	.175	.410
6.0	.105	.085	.067	.055	.051	.061	.082	.120	.175	.410
8.0	.040	.035	.030	.030	.038	.050	.077	.120	.175	.410
10.0	.025	.025	.025	.025	.025	.040	.070	.120	.175	.410





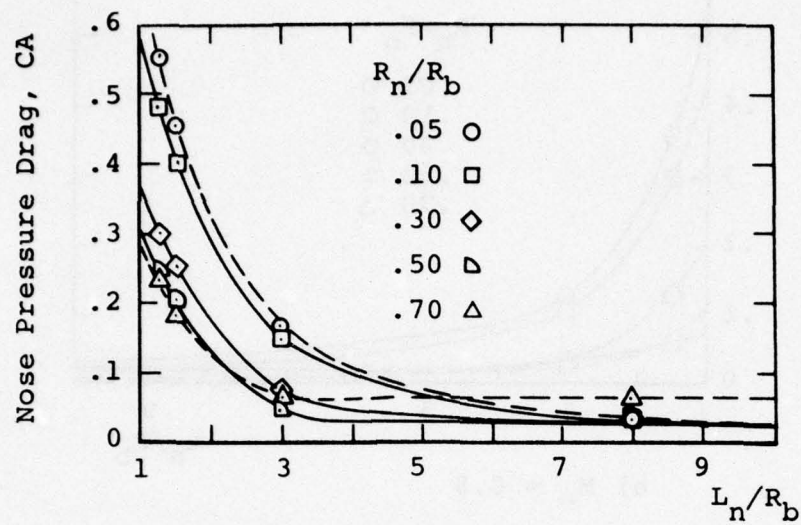


a)  $M_\infty = 0.8$

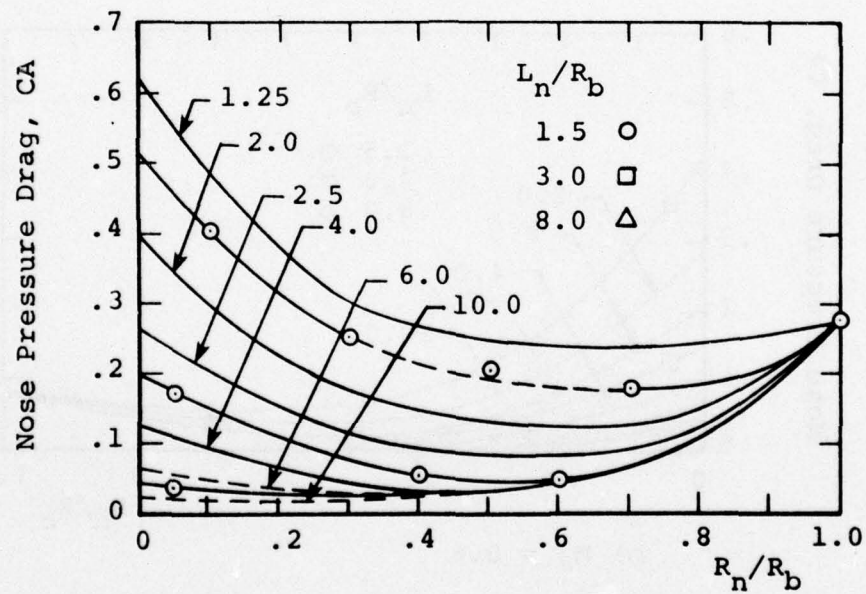


b)  $M_\infty = 0.8$

Figure 13. Calculated Values of Nose Pressure Drag Presented as a Function of Nose Length and Nose Bluntness for Varying Mach Numbers



c)  $M_\infty = 0.95$



d)  $M_\infty = 0.95$

Figure 13. Continued



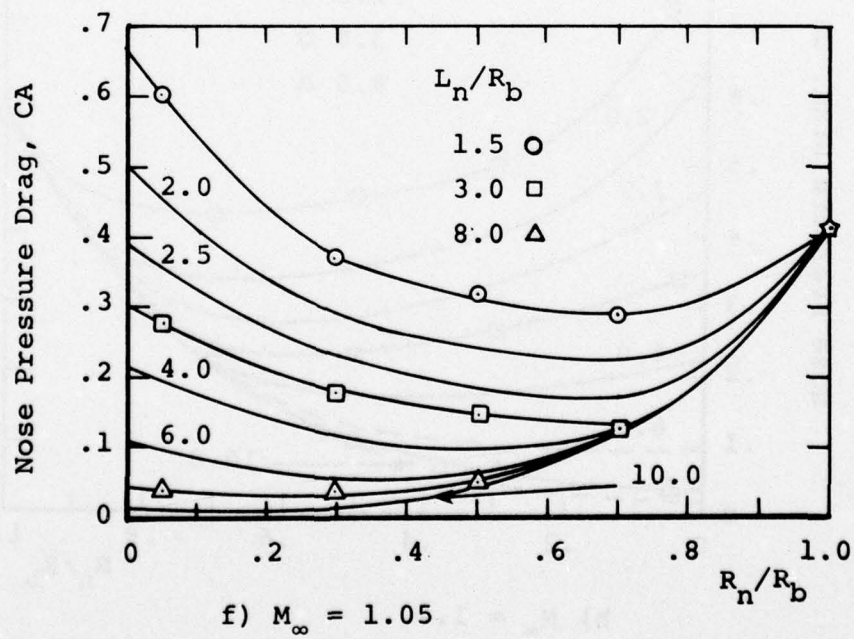
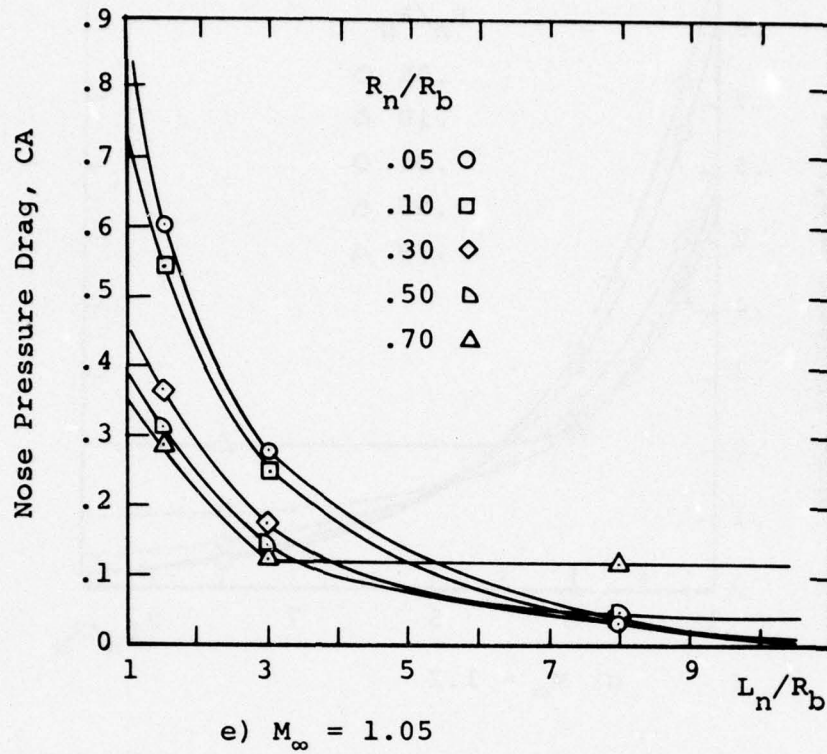


Figure 13. Continued

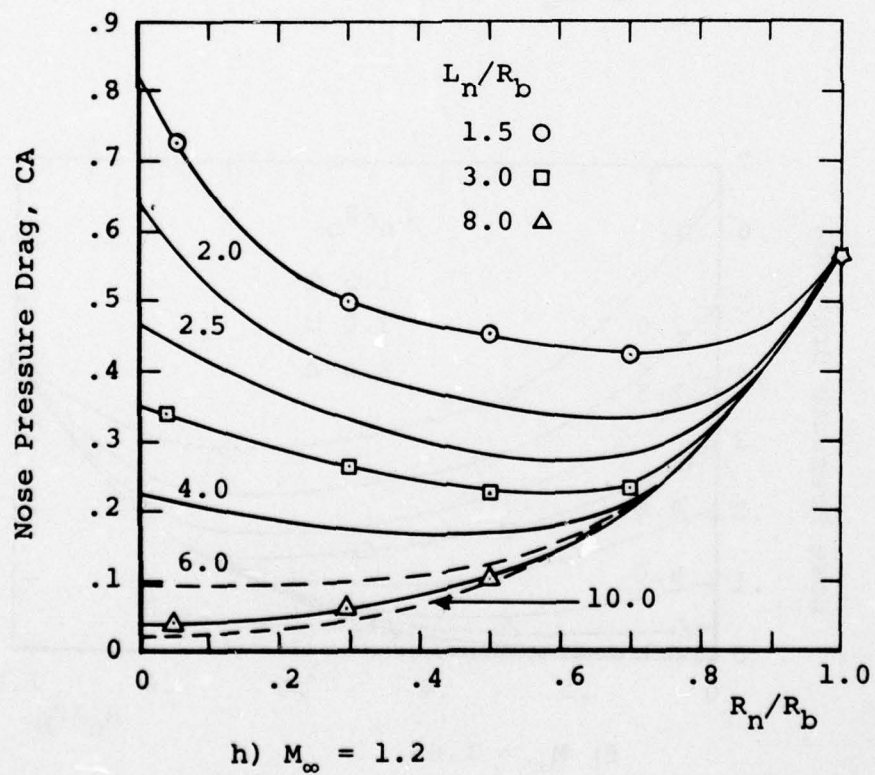
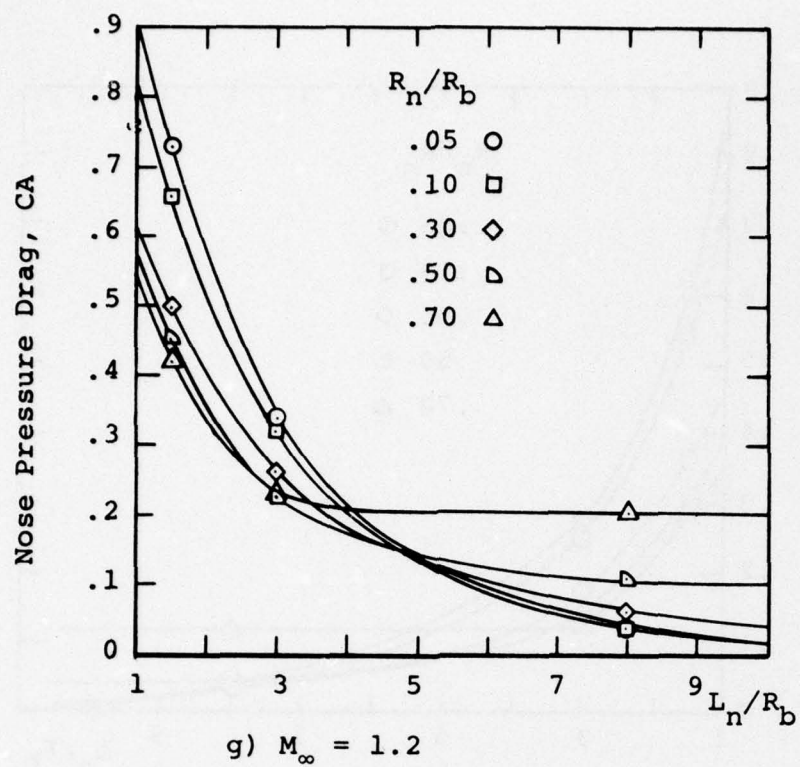


Figure 13. Concluded

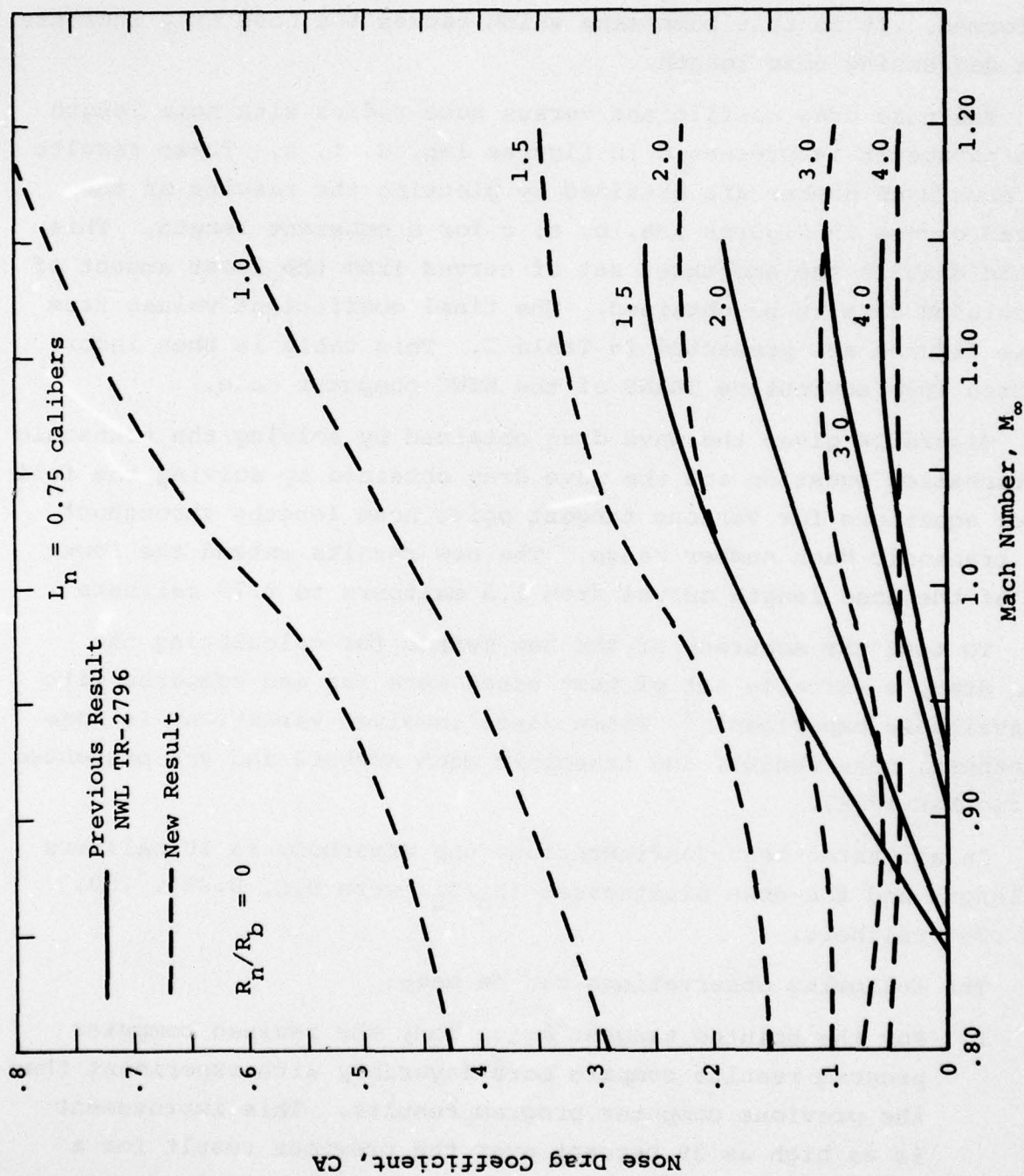


Figure 14. Transonic Wave Drag of Pointed Tangent Ogives for Various Nose Lengths in Calibers



rapidly increases with decreasing nose lengths when these lengths are less than 1.5 calibers. As the body becomes more blunt, the flow expands more rapidly and a larger pocket of supercritical flow is formed. It is this phenomena which causes the nose drag increase with decreasing nose length.

The nose drag coefficient versus nose radius with nose length as a parameter is presented in figures 13b, d, f, h. These results for each Mach number are obtained by plotting the results of the faired curves in figures 13a, c, e, g for a constant length. This method enables the smoothest set of curves from the least amount of calculated data to be obtained. The final coefficient values from these figures are presented in Table I. This table is then incorporated into subroutine TRANS of the NSWC computer code.

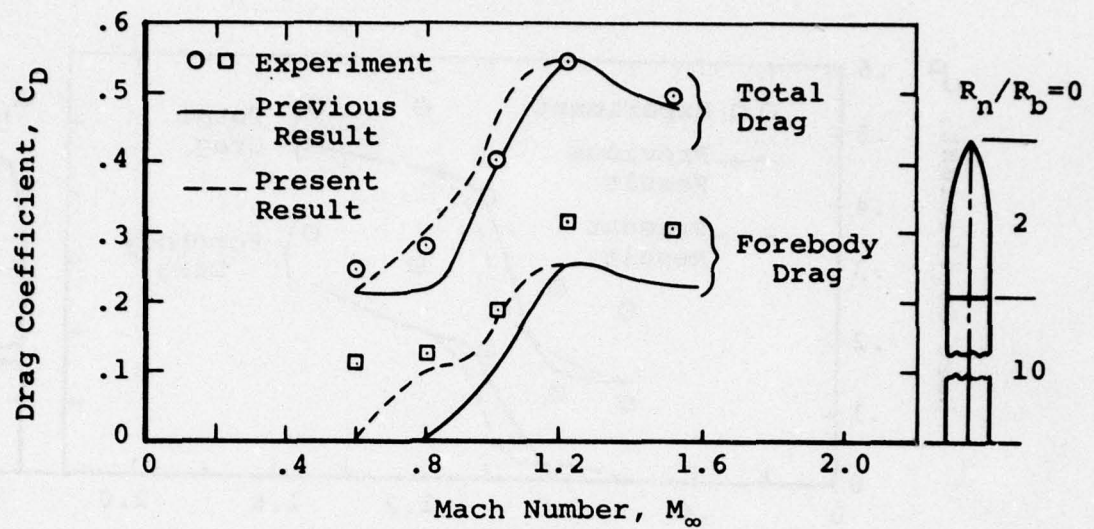
Figure 14 gives the wave drag obtained by solving the transonic perturbation equation and the wave drag obtained by solving the full Euler equations for various tangent ogive nose lengths throughout the transonic Mach number range. The new results extend the lower end of the nose length curves from 1.5 calibers to 0.75 calibers.

To test the accuracy of the new method for calculating the nose drag, a suitable set of test cases were run and compared with an available experiment.<sup>9</sup> These cases involved variations in nose bluntness, nose length, and transonic Mach numbers and are presented in figures 15-17.

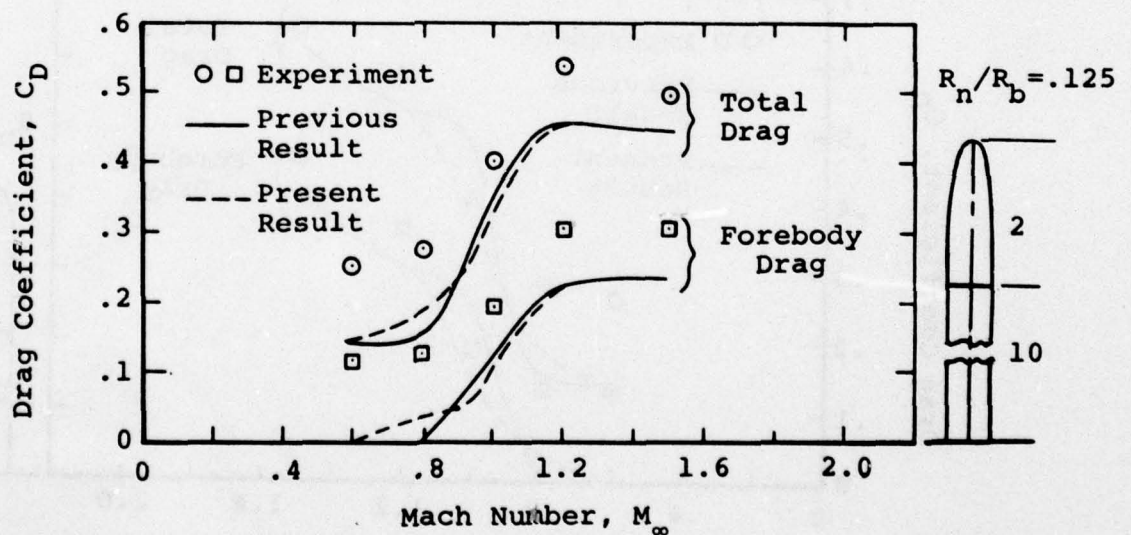
In all three test configurations the afterbody is 10 calibers in length and the nose bluntnesses ( $R_n/R_b$ ) were 0.0, 0.250, .50, and .750 calibers.

The following observations can be made:

1. For the pointed tangent ogive body the revised computer program results compare more favorably with experiment than the previous computer program results. This improvement is as high as 39 percent over the previous result for a pointed 2 caliber nose length projectile at a free stream  $M_\infty = 0.8$ .

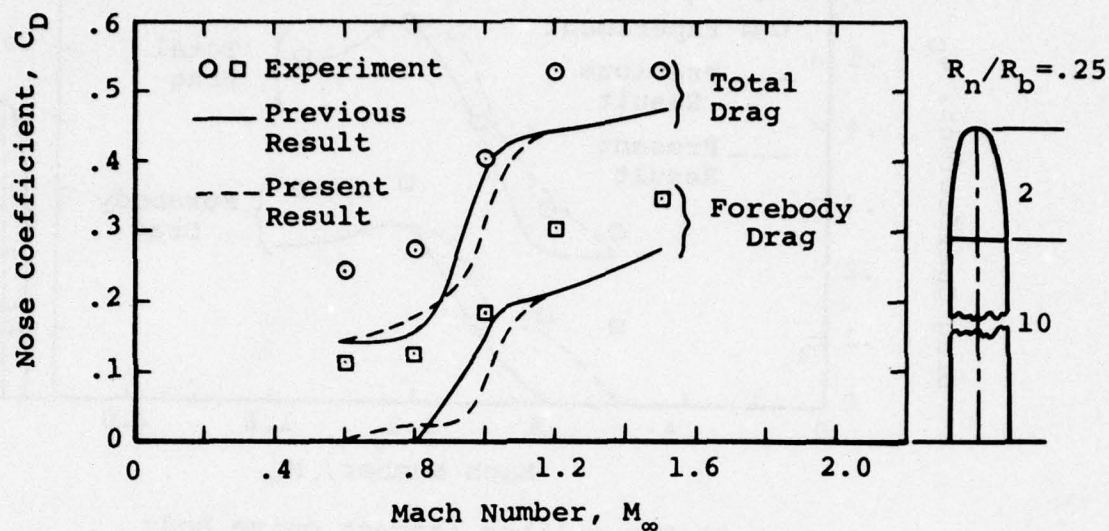


a) Two caliber tangent ogive body with a pointed nose.

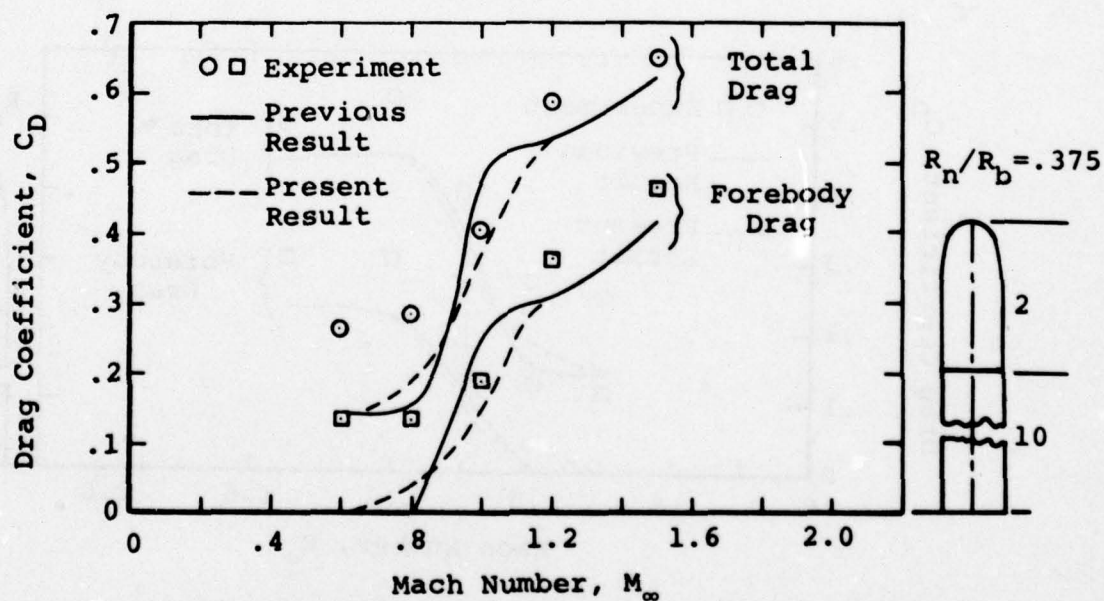


b) Two caliber tangent ogive body with a nose bluntness of .125.

Figure 15. Total and Forebody Drag Comparisons of the Present and Previous Theoretical Results with Experiment



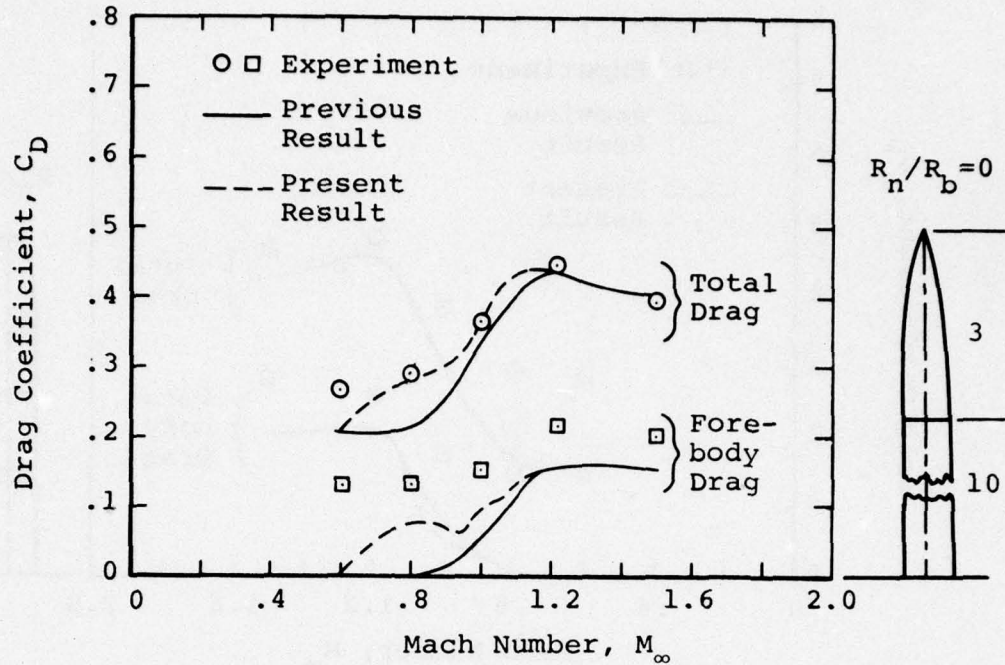
c) Two caliber tangent ogive body with a nose bluntness of 0.25



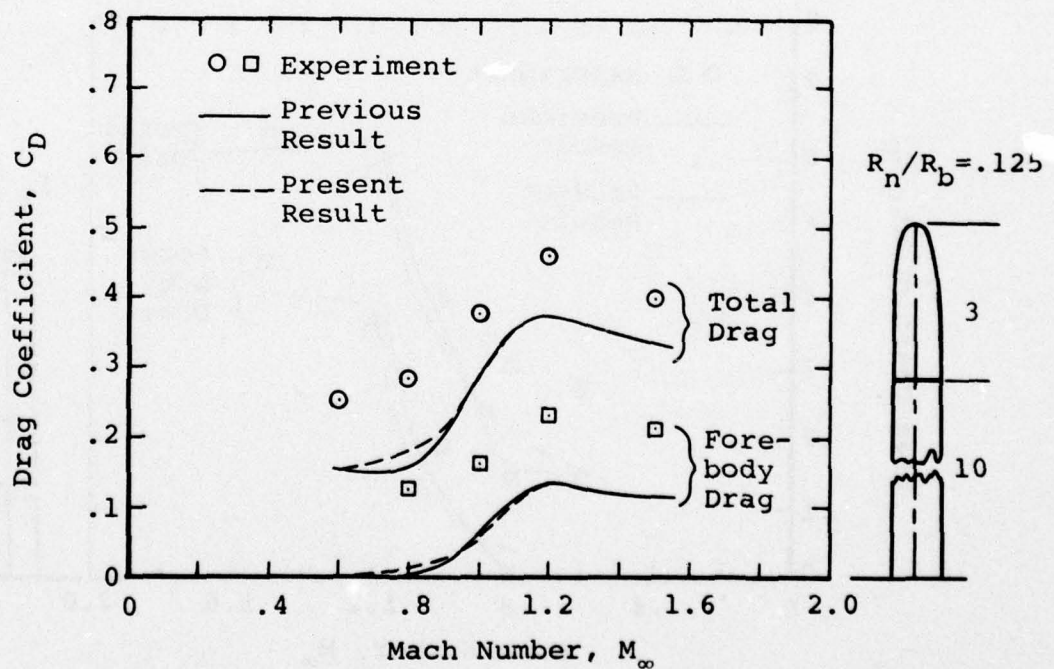
d) Two caliber tangent ogive body with a nose bluntness of 0.375

Figure 15. Concluded



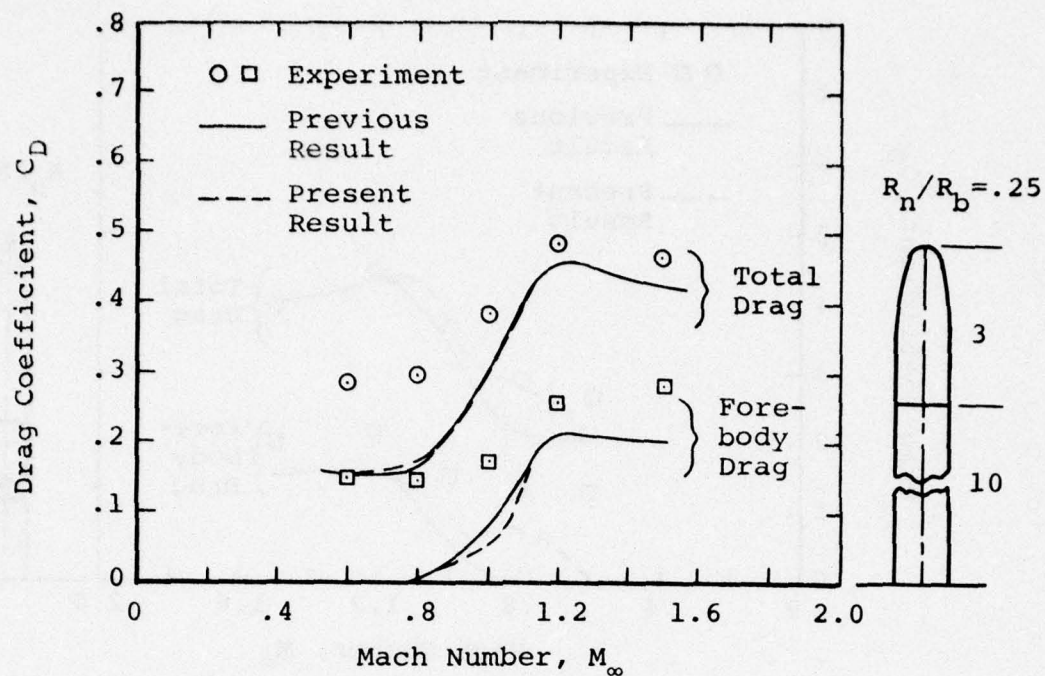


a) Three caliber tangent ogive body with a pointed nose

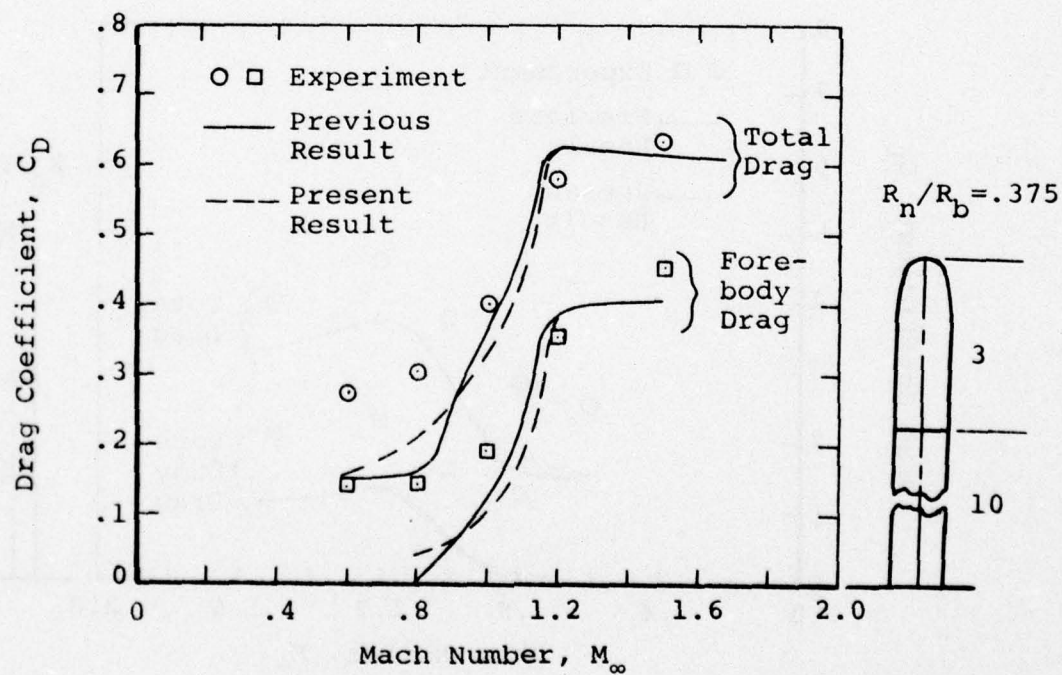


b) Three caliber tangent ogive body with a nose bluntness of 0.125

Figure 16. Total and Forebody Drag Comparisons of the Present and Previous Theoretical Results with Experiment

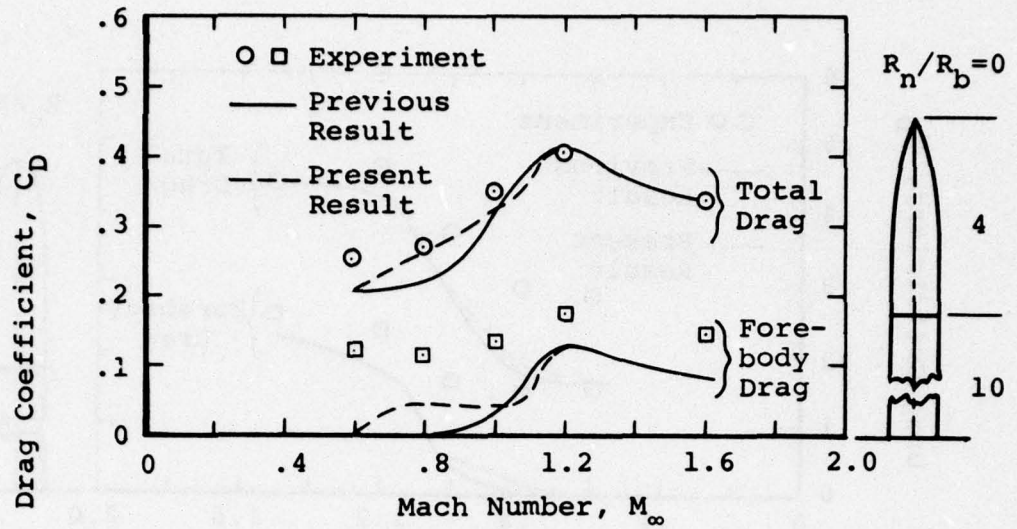


c) Three caliber tangent ogive body with a nose bluntness of 0.25

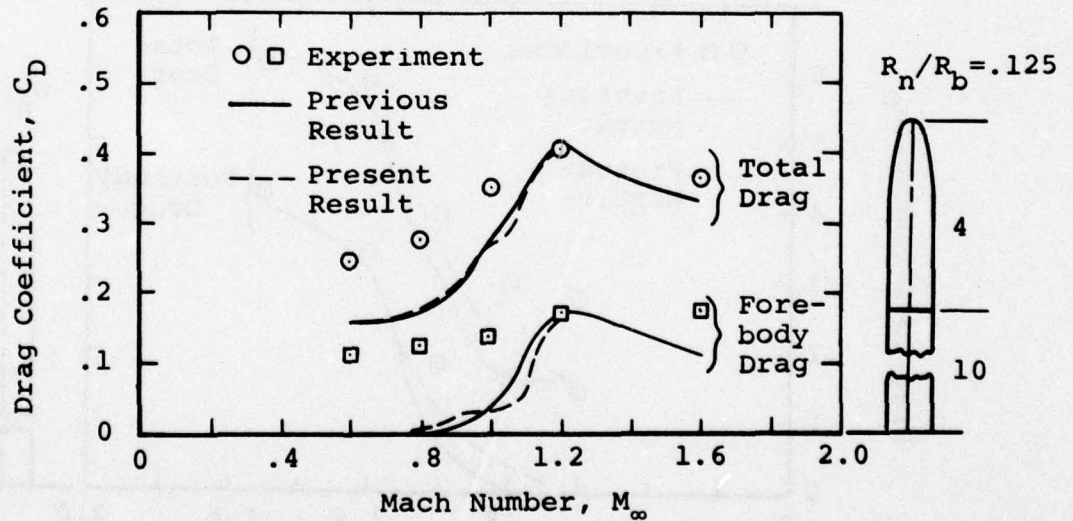


d) Three caliber tangent ogive body with a nose bluntness of 0.375

Figure 16. Concluded



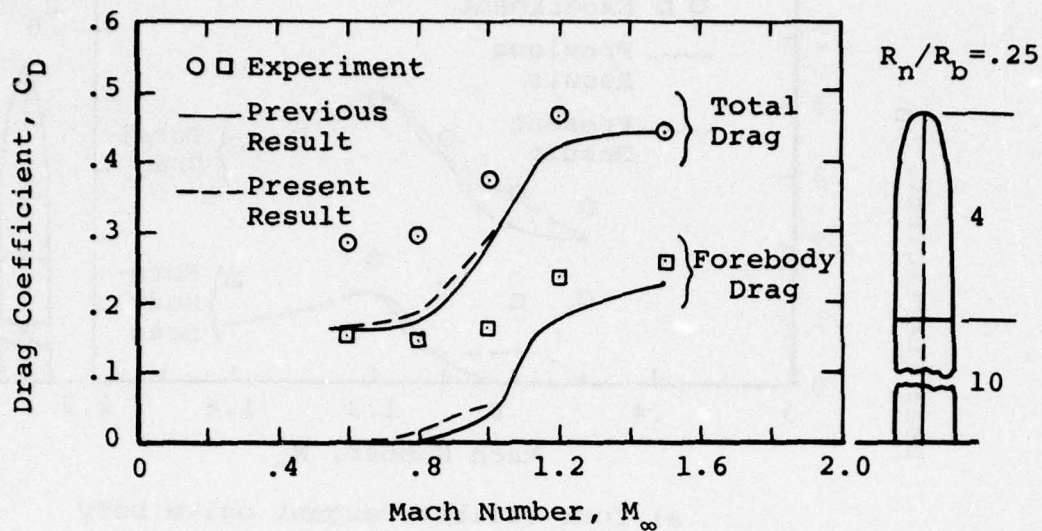
a) Four caliber tangent ogive body with a pointed nose



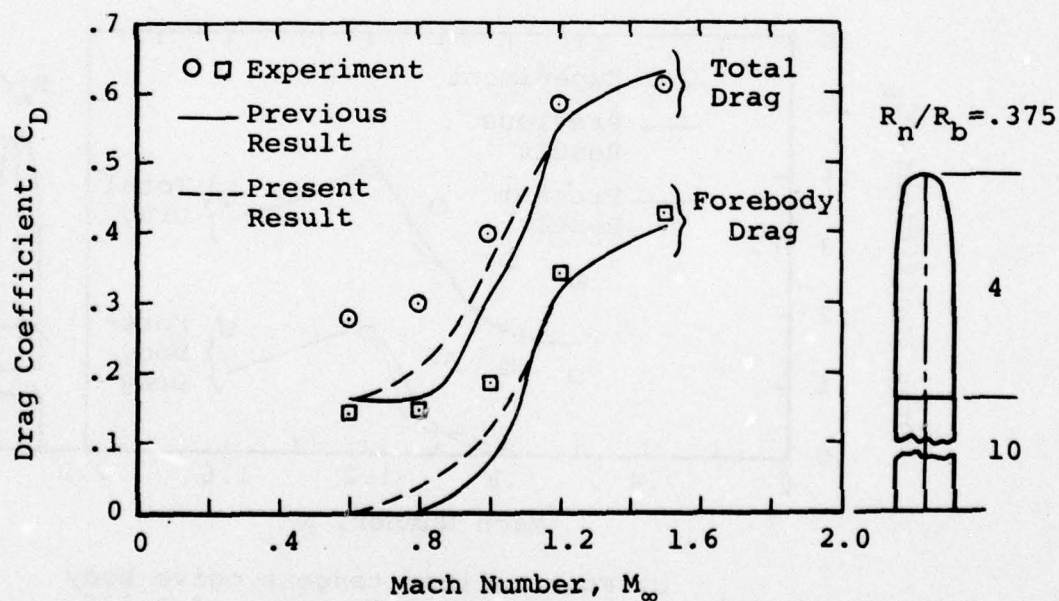
b) Four caliber tangent ogive body with a nose bluntness of 0.125

Figure 17. Total and Forebody Drag Comparisons of the Present and Previous Theoretical Results with Experiment





c) Four caliber tangent ogive body with a nose bluntness of 0.25



d) Four caliber tangent ogive body with a nose bluntness of 0.375

Figure 17. Concluded

2. For the larger nose bluntnesses the revised computer program results again compare more favorably with experiment than the previous results. The maximum improvement of 27 percent occurs at a free stream  $M_\infty = 0.8$ , a nose bluntness,  $R_n/R_b = .375$ , and a nose length  $L_n/2R_b = 4$ .
3. For transonic Mach numbers less than 0.85 the revised computer program gives results which are closer to experiment.
4. The experimental points were obtained in laminar flow whereas the calculations are performed assuming turbulent flow. This could explain the discrepancy between the theory and the experiment.

### Computer Program Alterations

There have been no changes in the input/output portions of the NSWG code. The changes in TRANS and MAIN, and the additional subroutines necessary are documented below.

#### INTERD, INTER3

These subroutines are used to interpolate for the value of a function at a given point. Three point Lagrange interpolation is used.

```
SUBROUTINE INTERD(TX,TY,X,Y,N,J)
DIMENSION TX(100),TY(100)
I=0
I=I+1
IF(TX(I) .LE. X)GO TO 1
IF(I .LE. J)I=J
IF(I .GT. (N-1))I=N-1
CALL INTER3(X,TX(I-1),TX(I),TX(I+1),TY(I-1),TY(I),TY(I+1),Y)
RETURN
END
```

```
      SUBROUTINE INTER3(X,X1,X2,X3,F1,F2,F3,F)
C.....3 POINT LAGRANGE INTERPOLATION FORMULA
C.....X1 .LE. X .LE. X3
      A1=(X-X2)*(X-X3)
      A2=(X-X1)*(X-X3)
      A3=(X-X1)*(X-X2)
      D1=(X1-X2)*(X1-X3)
      D2=(X2-X1)*(X2-X3)
      D3=(X3-X1)*(X3-X2)
      C1=A1/D1
      C2=A2/D2
      C3=A3/D3
      F=C1*F1+C2*F2+C3*F3
      RETURN
      END
```

THIS PAGE IS BEST QUALITY PRACTICABLE  
FROM COPY FURNISHED TO DDG



The changes in TRANS are shown by a solid line down the left hand margin. A sample input data sheet is shown in figure 18 where an accompanying sketch with the geometric parameters describing the configuration is also given. Figure 19 gives the sample output for the test case.  $C_D$  for  $0.5 < M_\infty < 0.8$  is reduced quadratically to zero from a table value at  $M_\infty = 0.8$ . This and other improved modifications to program changes in the original NEAR TR 153 were made by L. Devan at NSWC.

#### CONCLUSIONS AND RECOMMENDATIONS

1. An accurate implicit axisymmetric Euler equation solver has been used to obtain nose drag coefficients for transonic flow over sphere ogive cylinders.

2. A matrix of drag values was calculated for the following parameters

$$0.8 \leq M_\infty \leq 1.2$$

$$0 \leq R_n/D \leq .5$$

$$.75 \leq L_n/D \leq 10$$

3. The computed matrix was incorporated into the NSWC computer code as a table lookup. Several test cases were run and compared with experiment.

4. It is recommended the Euler equation solver be used to calculate drag coefficients for bodies with surface discontinuities, and be used to calculate drag coefficients for sphere-ogive bodies in the Mach number range 0.5 to 0.8.

THIS PAGE IS BEST QUALITY PRACTICABLE  
FROM COPY FURNISHED TO DDG

```

CHANGE OCCURS AT MAIN.8
COMMON/GE04/K,F,RR,RREF
COMMON/GE04/K,F,RR,RREF,TH1
CHANGE OCCURS AT MAIN.326
CA4=J.3
GO TO 5
GO TO 2
51 CA4=0.012*(THE1-10.)
GO TO 5
GO TO 2
19 IF(VOVS. LT. 1.19) GO TO 2
CALL HYBRID
GO TO 5
CALL TRANS
2 IF(VOVS. LE. .51)GO TO 5
CALL TRANS
CHANGE OCCURS AT BASEP.6
COMMON/GE04/K,F,RR,RREF
COMMON/GE04/K,F,RR,RREF,TH1
CHANGE OCCURS AT BLUNT.6
COMMON/GE04/K,F,RR,RREF
COMMON/GE04/K,F,RR,RREF,TH1
CHANGE OCCURS AT GEOM.6
COMMON/GE04/K,F,RR,RREF
COMMON/GE04/K,F,RR,RREF,TH1
CHANGE OCCURS AT HYBRID.6
COMMON/GE04/K,F,RR,RREF
COMMON/GE04/K,F,RR,RREF,TH1
CHANGE OCCURS AT NEWT.6
COMMON/GE04/K,F,RR,RREF
COMMON/GE04/K,F,RR,RREF,TH1
CHANGE OCCURS AT NORMFO.6
COMMON/GE04/K,F,RR,RREF
COMMON/GE04/K,F,RR,RREF,TH1
CHANGE OCCURS AT SIMP.6
COMMON/GE04/K,F,RR,RREF
COMMON/GE04/K,F,RR,RREF,TH1
CHANGE OCCURS AT SKINF.6
COMMON/GE04/K,F,RR,RREF
COMMON/GE04/K,F,RR,RREF,TH1
SUBROUTINE TRANS
COMMON/GEOM/ RP(6),X(30),R(30),C2,N,VSHAPE,N1,N2,XR(225),RB(225)
COMMON/GE01/ RBP(225),PETA
COMMON/GE02/ NN1,NN2,NN3,NN4,NFL,NB_JNT,NV,NNI,IPRINT,NN1A
COMMON/GE03/ VOVS,AL,XM,YM,XINT,YINT,NN1A
COMMON/CPV/ CPV(225,7),JA,JB
COMMON/GE04/K,F,RR,RREF,TH1
COMMON/DIS2/ SUM1,SUM2,SUM3,SUM4,SJ45,SJ46,CABLW
COMMON/LENG/ BL,ANL,ALA
COMMON/WAVE/ CABL,CN3L,CM3L,CAW,CNW,CMW
DIMENSION CA15(4,10),CA2(4,10),CA25(4,10),CA3(4,10),CA4(4,10),
) CA6(4,10),CA8(4,10),CA10(4,10),CA15R(4),CA2 R(4),AM(4),
) CA3 R(4),CA4 R(4),CA6 R(4),CA8 R(4),CA10R(4),CD(10),
) AO(10),A1(10),A2(10),A3(10),A4(10),A5(10),A6(10),A7(10)
DIMENSION CA25R(4)
DATA (AM(I),I=1,4) / .8,.35,1.05,1.2/
DATA ((CA15(I,J),I=1,4),J=1,10)/.422,.518,.67,.82,.29,.4,.541,.652,
).198,.311,.441,.552,.130,.250,.365,.497,.089,.211,.335,.47,.065,
).19,.31,.451,.06,.18,.291,.435,.051,.18,.285,.425,.06,.184,.3,.435
).,08,.278,.41,.565/
DATA ((CA2 (I,J),I=1,4),J=1,10)/.29,.395,.505,.64,.2,.295,.409,.521
).,13,.223,.339,.45,.081,.175,.29,.404,.051,.144,.26,.374,.04,.13,
).24,.35,.04,.123,.229,.335,.045,.128,.223,.333,.055,.15,.24,.355.

```



```

) .08,,278,,41,,565/
  DATA((CA25(I,J),I=1,4),J=1,10)/.213,.262,.39,.468,.14,.2,.321,.411
) .088,.15,.27,.37,.051,.115,.23,.333,.03,.091,.202,.302,.02,.08,
) .18,.281,.022,.081,.17,.27,.031,.031,.17,.28,.042,.121,.2,.32,.08,
) .278,.41,.565/
  DATA((CA3 (I,J),I=1,4),J=1,10)/.151,.198,.302,.350,.101,.15,.25,
) .319,.065,.11,.21,.29,.035,.075,.19,.253,.02,.055,.16,.245,.018,
) .047,.145,.231,.022,.049,.135,.23,.031,.065,.13,.24,.042,.108,
) .175,.302,.08,.278,.41,.565/
  DATA((CA4 (I,J),I=1,4),J=1,10)/.1,.130,.211,.225,.070,.091,.175,
) .205,.04,.061,.14,.19,.02,.042,.115,.175,.01,.04,.1,.17,.01,.031,
) .095,.17,.02,.048,.1,.18,.031,.065,.121,.211,.042,.108,.175,.29,
) .08,.278,.41,.565/
  DATA((CA6 (I,J),I=1,4),J=1,10)/.068,.080,.105,.095,.041,.049,.085,
) .092,.02,.038,.067,.095,.007,.032,.055,.1,.006,.031,.051,.109,.01,
) .031,.061,.121,.02,.048,.082,.151,.031,.065,.12,.205,.042,.108,
) .175,.29,.08,.278,.41,.565/
  DATA((CA8 (I,J),I=1,4),J=1,10)/.05,.04,.04,.04,.029,.031,.035,.04,
) .012,.021,.03,.05,.007,.028,.03,.06,.006,.028,.038,.07,.01,.031,.05,
) .105,.02,.048,.07,.145,.031,.065,.12,.204,.042,.108,.175,.29,.08,
) .278,.41,.565/
  DATA((CA13(I,J),I=1,4),J=1,10)/.041,.025,.025,.025,.02,.020,.025,.025,
) .008,.015,.025,.03,.007,.020,.025,.041,.006,.021,.025,.055,.01,.031,
) .04,.095,.02,.048,.07,.14,.031,.065,.12,.204,.042,.108,.175,.29,
) .08,.278,.41,.565/
  C83=0.
  IF(R3P(NN).LT.-C.0001) GO TO 87
  GO TO 88
87 VOV=VOVS-.0498
  IF(VOV.LT.1.) GO TO 89
  AREF=3.14159*RRF**2
  IF(NSHAPE.LT.4) GO TO 98
  IF(NN1A.EQ.2) GO TO 1
  IF(N3LUNT.EQ.2) GO TO 1
  J=NV2+1
  GO TO 2
1 J=NV3+1
2 DO 10 L=J,NN
  XX=YB(L)-XB(J)
  DELTA=ATAN(1./(2.*ANL))
  IF(R3P(J-3).LT.R3P(1)) DELTA=ATAN(.2/ANL)
  GAMMA=1.4
  C1=1.+GAMMA
  C0=SQRT(C1)
  C3=VOV **2
  C4=1.-C3
  C5=C4/(C1*C3)
  C6=3.*DELTA/(2.*C5)
  C7=25.*C1*VOV ** (2./3.)
  C8=.5*C4/(C1*C3)
  C9=1.25*C5**2
  C10=2.*C5/(VOV ** (2./3.))*C6** (2./3.)
  C11=(C6/VOV )** (4./3.)
  CS7=C7*(C8+(C9+C10+C11)** (.5))
  CSQRT(CS7)
  Y=2.*ALA +2.*XX
  CP1 =.4*(Y-C)/SQRT(C1*VOV ** (2./3.))* (.04*(Y-C)**2/(C1*VOV **
1 (2./3.))-C4/(C1*C3))**.5
  IF(Y.GT.C) CP1=0.
  DELTA=-RBP(L)
  GAMMA=1.4
  C1=1.+GAMMA
  C0=SQRT(C1)
  C3=VOV **2
  C4=1.-C3
  C5=C4/(C1*C3)

```



THIS PAGE IS BEST QUALITY PRACTICABLE  
FROM COPY FURNISHED TO DDC

```

C6=3.*DELTA/(2.*C0)
C7=25.*C1*VOV ** (2./3.)
C8=.5*C4/(C1*C3)
C9=1.25*C5**2
C10=2.*C5/(VOV ** (2./3.))*C6** (2./3.)
C11=(C6/VOV )** (4./3.)
CSQ=C7*(C8+(C9+C10+C11)** (.5))
C=SQR(CSQ)
Y=XX*2.
CPV(L, 1)=.4*(Y-C)/SQR(C1*VOV ** (2./3.))* (.04*(Y-C)**2/(C1*VOV **
1(2./3.))-C4/(C1*C3))** .5-DELTA**2+>1
IF(Y.GT.C) CPV(L,1)=CP1
15 DO 10 K1=1,7
   CPV(L,K1)=CPV(L,1)
10 CONTINUE
   JA=J
   JB=NN
   SUM1=0.
   SUM2=0.
   SUM3=0.
   CALL SIMP
   C80=2.*SUM1/AREF
   V0=VOV-1.
   IF(V0.LE.0.06) C81=C80
   V1=VOVS
89 CONTINUE
   IF(VOVS.GT.0.95) GO TO 90
   C83=0.
   GO TO 88
90 C80=C81*(VOVS-.95)/(V1-.95)
88 CONTINUE
C.....TABLE LOOKUP IS BASED ON LN/RB, RN/RB
   ANL1=ANL
   ANL=ANL+RR*(-1.+1./(1.+SIN(TH1)))
   ANL=2.*ANL
   VV=VOVS
   IF(VOVS. LT. .8) VOVS=.8
C
C*****
C
C DETERMINE RNORB, THE CORRECT RADIUS OF THE NOSE, TO
C BE USED IN TABLE LOOKUP.
C
C RNORB=2.0*R(1)/COS(TH1)
C*****
C
C WRITE(6,200) VOVS,ANL,RNORB
200 FORMAT(* *,*MACH NO., NOSE LENGTH, RN/RB*,3F15.10,///
1 * AS AND DRAG*)
   IF(ANL.GT.10.) ANL=10.
   IF(ANL. LT. 1.5) ANL=1.5
   IF(RNORB.GE.0.4) GO TO 21
   J1=1
   J2=5
   GO TO 22
21 IF(RNORB.LE.0.5) GO TO 23
   J1=5
   J2=10
   GO TO 22
23 J1=4
   J2=8
22 DO 14 J=J1,J2
   DO 13 I=1,4
   IF(ANL.GT.4.) GO TO 24
   CA15R(I)=CA15(I,J)

```

```

      CA2 R(I)=CA2 (I,J)
      CA25R(I)=CA25(I,J)
24    CA3R(I)=CA3(I,J)
      CA4 R(I)=CA4 (I,J)
      IF(ANL.LE.4.) GO TO 13
      CA6 R(I)=CA6 (I,J)
      CA8 R(I)=CA8 (I,J)
      CA10R(I)=CA10(I,J)
13    CONTINUE
      IF(ANL.GT.4.) GO TO 26
19    CALL INTER5(RNORR,.3,.4,.5,.6,.7,C)(4),CD(5),CD(6),CD(7),CJ(8),
      )
      CALL INTERD(AM,CA15R,VOVS,A0(J),4,2)
      CALL INTERD(AM,CA2 R,VOVS,A1(J),4,2)
      CALL INTERD(AM,CA25R,VOVS,A2(J),4,2)
26    CALL INTERD(AM,CA3 R,VOVS,A3(J),4,2)
      CALL INTERD(AM,CA4 R,VOVS,A4(J),4,2)
      IF(ANL.LE.4.) GO TO 25
      CALL INTERD(AM,CA6 R,VOVS,A5(J),4,2)
      CALL INTERD(AM,CA8 R,VOVS,A6(J),4,2)
      CALL INTERD(AM,CA10R,VOVS,A7(J),4,2)
      GO TO 12
25    CALL INTER5(ANL,1.5,2.,2.5,3.,4.,A0(J),A1(J),A2(J),A3(J),A4(J),
      )
      )
      GO TO 14
12    CALL INTER5(ANL,3.,4.,6.,8.,10.,A3(J),A4(J),A5(J),A6(J),A7(J),
      )
      )
      GO TO 14
14    CONTINUE
      IF(RNORR .GE. 0.4)GO TO 16
      CALL INTER5(RNORR,0.,.1,.2,.3,.4,C)(1),CJ(2),CD(3),CD(4),CD(5),
      )
      )
      GO TO 17
16    IF(RNORR .LE. 0.5)GO TO 19
      CALL INTER5(RNORR,.5,.6,.7,.8,1.,C)(6),CJ(7),CD(8),CD(9),CJ(10),
      )
      )
      GO TO 17
17    IF(VV .GE..8)GO TO 18
      CAN=CAN*((VV-.5)/.3)**2
      VOVS=VV
18    CAW=CAN+C80+CAW
      WRITE(6,215) CAN,CAW
215  FORMAT(* *,*NOSE DRAG AND WAVE DRAG*,2F15.10)
      ANL=ANL1
99    RETURN
      END
CHANGE OCCURS AT WAVE.8
COMMON/GE04/K,F,RR,RREF
COMMON/GE04/K,F,RR,RREF,TH1

```

THIS PAGE IS BEST QUALITY PRACTICABLE  
FROM COPY FURNISHED TO DDC





CASE NO. 1

ANGLE OF ATTACK = 0.00DEGS

REFERENCE DIAMETER = 1.000FT

REFERENCE CONDITIONS

SPEED OF SOUND = 1116.890 FT/SEC  
DENSITY = .0023769 SLUGS/FT<sup>3</sup>  
ABSOLUTE VISCOSITY = .000000374528 LB-SEC/FT<sup>2</sup>  
MOMENT REFERENCE = 0.00CALIBERS FROM NOSE TIP

BODY COORDINATES

X	R
0.0000	0.0000
.1250	.0450
.2500	.0800
.3750	.1200
.5000	.1550
.6250	.1900
.7500	.2250
.8750	.2500
1.0000	.2800
1.1250	.3100
1.2500	.3350
1.3750	.3600
1.5000	.3800
1.6250	.4000
1.7500	.4200
1.8750	.4300
2.0000	.4500
2.1250	.4600
2.2500	.4750
2.3750	.4800
2.5000	.4850
2.6250	.4900
2.7500	.4950
2.8750	.4975
3.0000	.5000
4.0000	.5000
6.0000	.5000
8.0000	.5000
10.0000	.5000

Figure 19. Sample Output for Tangent Ogive Configuration  
of Figure 18

THIS PAGE IS BEST QUALITY PRACTICABLE  
FROM COPY FURNISHED TO DDC

### BODY AXIAL FORCE CONTRIBUTIONS

MACH NO.	SKIN FRICTION	BASE PRESSURE	PRESSURE	PROTRUSIONS	TOTAL
1.500	.0633	.1910	.1504	0.0000	.4046
1.200	.0681	.2180	.1524	0.0000	.4384
1.050	.0708	.2190	.1151	0.0000	.4048
1.000	.0717	.2090	.0963	0.0000	.3770
.950	.0726	.1844	.0660	0.0000	.3231
.800	.0755	.1350	.0767	0.0000	.2872
.600	.0798	.1285	.0085	0.0000	.2168

### TOTAL STATIC AERODYNAMICS (FORCE/ALPHA)

MACH NO.	CD	CN	CL	CM	CNAL	CMAL XCP/D
1.500	.4046	0.0000	0.0000	0.000	0.000	0.0000.0000
1.200	.4384	0.0000	0.0000	0.000	0.000	0.0000.0000
1.050	.4048	0.0000	0.0000	0.000	0.000	0.0000.0000
1.000	.3770	0.0000	0.0000	0.000	0.000	0.0000.0000
.950	.3231	0.0000	0.0000	0.000	0.000	0.0000.0000
.800	.2872	0.0000	0.0000	0.000	0.000	0.0000.0000
.600	.2083	0.0000	0.0000	0.000	0.000	0.0000.0000

### CONFIGURATION DYNAMIC DERIVATIVES

MACH NO.	CLP	CMQ+CMAD	CNPA1	CNPA5
1.50	-.042	-369.240	0.000	0.000
1.20	-.042	-369.240	0.000	0.000
1.05	-.043	-369.240	0.000	0.000
1.00	-.044	-369.240	0.000	0.000
.95	-.046	-369.240	0.000	0.000
.80	-.066	-369.240	0.000	0.000
.60	-.066	-369.240	0.000	0.000

Figure 19. Concluded



## REFERENCES

1. F. G. Moore and R. C. Swanson, *Aerodynamics of Tactical Weapons to Mach Number 3 and Angle of Attack 15°*. Part I - Theory and Application, NSWC/DL TR-3584, Feb. 1977. Part II - Computer Program and Usage, NSWC/DL TR-3600, Mar. 1977.
2. K. Aoyama and J. M. Wu, *On Transonic Flow Field Around Tangent Ogive Bodies*, AIAA Paper 70-189, presented at AIAA 8th Aerospace Sciences Meeting, New York, N.Y., Jan. 19-21, 1970.
3. D. S. Chaussee, S. S. Stahara, and J. R. Spreiter, *Application of an Axisymmetric Implicit Blunt Body Procedure: "Computation of Solar Wind Flows Past Terrestrial Planets,"* AIAA Paper 77-700 presented at the AIAA 10th Fluid and Plasma Dynamics Conference, Albuquerque, New Mexico, June 27-29, 1977.
4. R. M. Beam and R. F. Warming, *An Implicit Finite-Difference Algorithm for Hyperbolic Systems in Conservation-Law Form*, J. Comp. Phys., Vol. 22, no. 1, Sept. 1976.
5. D. S. Chaussee, *On the Transonic Flow Field Surrounding Tangent-Ogive Bodies with Emphasis on Nose Drag Calculations*, AIAA Paper 78-212, to be presented at AIAA 16th Aerospace Sciences Meeting, Huntsville, AL, January 16-18, 1978.
6. C. P. Kentzer, *Discretization of Boundary Conditions on Moving Discontinuities*, Proceedings of the Second International Conference on Numerical Methods in Fluid Dynamics, Lecture Notes in Physics, Vol. 8, edited by M. Holt, Berkeley, CA, September 15-19, 1970, pp. 108-113.
7. P. D. Thomas, M. Vinokur, R. Bastionon, and R. J. Conti, *Numerical Solution for the Three-Dimensional Hypersonic Flow Field of a Blunt Delta Body*, AIAA Journal, Vol. 10, no. 7, July 1972, pp. 887-894.
8. T. Hsieh, *Flow Field Study About a Hemisphere Cylinder in Transonic and Supersonic Mach Number Range*, AIAA Paper 75-83, presented at AIAA 13th Aerospace Sciences Meeting, Pasadena, CA, January 20-22, 1975.



9. C. B. Butler, E. Sears, and S. G. Pallas, *Aerodynamic Characteristics of 2, 3 and 4-Caliber Tangent-Ogive Cylinders with Nose Bluntnesses of 0.00, 0.25, 0.50 and 0.75, at Mach Numbers from 0.6 to 4.0*, AFATL TR 77-8, January 1977.

# GLOSSARY OF TERMS

A	Jacobian matrix defined in Equation 4, $= \frac{\partial \hat{E}}{\partial \hat{u}}$
B	Jacobian matrix defined in Equation 4, $= \frac{\partial \hat{F}}{\partial \hat{u}}$
c	speed of sound $= (\gamma p / \rho)^{1/2}$
$C_D$	drag coefficient
$C_p$	pressure coefficient
dy	space increment
dt	time increment
D	drag
e	energy per unit volume
E	matrix of conservative variables defined in Equation 1
$\hat{E}$	$(\xi_t U + \xi_x E + \xi_y F) / J$
F	matrix of conservative variables defined in Equation 1
$\hat{F}$	$(\eta_t U + \eta_x E + \eta_y F) / J$
H	source matrix defined in Equation 1
I	identity matrix
j	$j = 0$ 2-D flow; $j = 1$ axisymmetric flow
J	Jacobian
$L_n$	length of nose
M	free stream Mach number
p	pressure
q	dynamic pressure $= \frac{1}{2} \rho_\infty q_\infty^2$
$q^2$	total velocity vector squared
$r_b, R_b$	radius of the cylindrical afterbody
$r_n, R_n$	radius of the spherical nose
S	smoothing term defined by Equation 7
$S_{ref}$	reference area $= \pi r_b^2$

$t$	time
$u$	velocity component in x-direction
$U$	matrix defined in Equation 1
$\hat{u}$	$U/J$
$v$	velocity component in y-direction
$x$	coordinate direction in physical plane
$y$	coordinate direction in physical plane
$y_b$	radius of the body
$Y$	term included in source term, $H$ of Equation 1
$\gamma$	ratio of specific heats, 1.4 in this study
$\delta$	central difference operator in Equation 6; shock angle in figure 8
$\epsilon$	smoothing coefficient, $0 \leq \epsilon \leq 0.4$
$\eta$	coordinate direction in computational plane
$\xi$	coordinate direction in computational plane
$\rho$	density
$\sigma$	eigenvalue defined in Equation 5
$\tau$	time
$\phi$	meridional angle defined in figure 2

#### Subscript

$b$	body
$i$	increment
$j$	$\xi$ -direction
$k$	$\eta$ -direction
$n, N$	nose

#### Superscript

$n$	time direction
(—)	averaging



DISTRIBUTION

Commander  
Naval Sea Systems Command  
Washington, DC 20360  
ATTN: SEA-03 (Mr. Lionel Pasiuk)  
Library (2)

Commander  
Naval Air Systems Command  
Washington, DC 20361  
ATTN: AIR-320 (Mr. Bill Volz)  
AIR-320 (Dr. H. Mueller)  
AIR-532  
Library (2)

Chief of Naval Research  
Arlington, VA 22217  
ATTN: Mr. Lawrence E. McCullough  
Mr. Dave Seigel  
Dr. Bob Whitehead  
Dr. R. J. Lundegard  
Mr. Mort Cooper  
Mr. Ralph Cooper  
Library (2)

Chief of Naval Operations  
Pentagon  
Washington, DC 20350  
ATTN: OP-098  
Library (2)

Commander  
Naval Material Command  
Washington, DC 20360  
ATTN: MAT-032 (Mr. Sid Jacobson)  
Dr. John Huth  
Library (2)

Commander  
Naval Weapons Center  
China Lake, CA 93555  
ATTN: Mr. Ray Van Aken  
Mr. D. Meeker  
Mr. Kinge-Okauchi  
Library (2)

Commander  
Pacific Missile Test Center  
Point Mugu, CA 93041  
ATTN: Mr. Joe Rom  
Library (2)

Commander  
David W. Taylor Naval Ship Research  
and Development Center  
Bethesda, MD 20084  
ATTN: Dr. T. C. Tai  
Library (2)

Commander  
Naval Air Development Center  
Warminster, PA 18974  
ATTN: Mr. Bill Langen  
Library (2)

Commanding Officer  
Naval Ordnance Station  
Indian Head, MD 20640

Commandant of the Marine Corps  
Headquarters, Marine Corps  
Washington, DC 20380

Commander  
Naval Air Engineering Center  
Aeronautical Structures Department  
Lakehurst, NJ 19112

Commander  
Naval Air Test Center  
Patuxent River, MD 20670  
ATTN: Mr. Ron Wilson  
Library (2)

Commander  
Naval Coastal Systems Laboratory  
Panama City, FL 32401 (2)

Commander  
Naval Ocean Systems Center  
San Diego, CA 92135 (2)

Commander  
Naval Underwater Systems Center  
Newport, RI 02480 (2)

Naval Research Laboratory  
Washington, DC 20375 (2)

Superintendent  
U. S. Naval Academy  
Annapolis, MD 21402  
ATTN: Head, Weapons Department  
Head, Science Department  
Library (2)

Superintendent  
U. S. Naval Postgraduate School  
Monterey, CA 95076  
ATTN: Head, Mechanical Engineering  
Department  
Head, Department of Aeronautics  
Library (2)

Chief of Naval Research  
Department of the Navy  
Washington, DC 20360

Director  
Naval Strategic Systems Projects  
Office (PM-1)  
Department of the Navy  
Washington, DC 20360 (2)

Officer in Charge  
U. S. Naval Scientific and  
Technical Intelligence Center  
U. S. Naval Observatory  
Washington, DC 20360 (2)

Commander  
Marine Corps Development and  
Education Command  
Quantico, VA 22134  
ATTN: Director, Development Center  
S&R Division  
Air Operations Division  
Ground Operations Division  
Library (2)

U. S. Army Armament Research and  
Development Command  
Dover, NJ 07801  
ATTN: Mr. E. F. Friedman  
Mr. Henry Hudgins  
Mr. M. Cline  
Mr. A. Loeb  
Mr. Mertz  
Library



Director, U. S. Army  
Ballistic Research Laboratory  
Aberdeen Proving Ground, MD 21005

ATTN: Dr. C. H. Murphy  
Mr. L. McAllister  
Mr. A. Platou  
Mr. B. McCoy  
Library

(2)

President  
U. S. Army Field Artillery Board  
Fort Sill, OK 73503  
ATTN: Marine Corps Liaison Officer  
Library

(2)

Commander  
U. S. Army Material Development and  
Readiness Command  
5001 Eisenhower Avenue  
Alexandria, VA 22333

Commander  
Frankford Arsenal  
Philadelphia, PA 19137  
ATTN: Mr. W. Gadomski  
Library

(2)

Commander  
Harry Diamond Laboratories  
2800 Powder Mill Road  
Adelphi, MD 20783  
ATTN: Technical Library

(2)

Commander  
U. S. Army Combat Development Command  
Field Artillery Agency  
Fort Sill, OK 73503

(2)

Commander  
U. S. Army Missile Command  
Redstone Arsenal, AL 35809  
ATTN: DRSMI (Mr. Ray Deep)  
DRSMI (Dr. D. J. Spring)  
Library

(2)

AF Office of Scientific Research  
Washington, DC 20330  
ATTN: Library

(2)

Headquarters  
Air Force Systems Command  
Andrews Air Force Base, MD 20331

Headquarters, USAF  
Washington, DC 20330

U. S. Air Force Systems Command  
Regional Offices  
c/o Department of the Navy  
Washington, DC 20360

Air Force Armament Laboratory  
Eglin Air Force Base, FL 32542

ATTN: Dr. D. Daniel  
Dr. S. G. Pallas  
Mr. C. Butler  
Dr. Lijewski  
Mr. C. Mathews  
Mr. K. Cobb  
Mr. E. Sears  
Library (2)

USAF Academy  
Colorado Springs, CO 80912 (2)

Air Development and Test Center  
Eglin Air Force Base, FL 32542 (2)

Arnold Engineering Development Center  
USAF  
Tullahoma, TN 37389  
ATTN: Mr. J. Usselton  
Mr. W. B. Baker, Jr.  
Library (2)

Edwards Air Force Base  
Edwards, CA 93523  
ATTN: Flight Research Center  
Rocket Propulsion Laboratory  
(Maj. Washburn)  
Library (2)

Wright Patterson Air Force Base  
Dayton, OH 45433  
ATTN: Aeronautical Systems Division (2)  
Aeronautical Research Laboratory  
Air Force Flight Dynamics  
Laboratory  
FGC (Mr. E. Flinn)  
(Dr. G. Kurylowich)  
(Dr. V. Hoehne)  
FX (Mr. Mel Buck)  
Library (2)

Advanced Research Projects Agency  
Department of Defense  
Washington, DC 20305

(2)

Director  
Defense Research and Engineering  
Department of Defense  
Washington, DC 20305  
ATTN: R&AT Office (Mr. B. Osborne)  
Library

(2)

Headquarters, NASA  
Washington, DC 20546

NASA George C. Marshal Flight Center  
Huntsville, AL 35804

NASA Goddard Space Center  
Greenbelt, MD 20771

NASA Lewis Research Center  
Cleveland, OH 44101

NASA Ames Research Center  
Moffett Field, CA 94035  
ATTN: Mr. Vic Peterson  
Mr. John Rakich  
Library

(2)

NASA Langley Research Center  
Langley Station  
Hampton, VA 23365  
ATTN: Dr. Roy C. Swanson, Jr.  
Mr. Bud Bobbitt  
Mr. Jerry South  
Mr. Leroy Spearman  
Mr. C. M. Jackson, Jr.  
Mr. W. C. Sawyer  
Library

(2)

Applied Physics Laboratory  
Johns-Hopkins University  
8621 Georgia Avenue  
Silver Spring, MD 20910  
ATTN: Dr. L. L. Cronvich  
Mr. Edward T. Marley  
Dr. Gordon Dugger  
Library

(2)



ARO Inc.  
Arnold Air Force Station, TN 37389  
ATTN: Dr. Tsuying Hsieh

Sandia Laboratories  
Albuquerque, NM 87115  
ATTN: Division 1331 (Mr. Robert LaFarge)  
Library

Sandia Laboratories  
Box 969  
Livermore, CA 94550  
ATTN: Division 8158  
Library

The Rand Corporation  
1600 Main Street  
Santa Monica, CA 90406

Stanford Research Institute  
Menlo Park, CA 94025  
ATTN: Dr. Milton Van Dyke  
Library

(2)

Raytheon Company  
Spencer Laboratory  
Burlington, MA 01803  
ATTN: BOX SL 7162 (Mr. Steve Pearlsing)

McDonnell Douglas Astronautics Co. (West)  
5301 Bolsa Avenue  
Huntington Beach, CA 92647  
ATTN: Mail Station 13-2 (Dr. Jim Zerikos)

Vought Corporation  
P. O. Box 5907  
Dallas, TX 75222  
ATTN: Dr. W. B. Brooks  
Mr. F. Prilliman

Boeing Computer Services, Inc.  
P. O. Box 24346, M/S 8F-37  
Seattle, WA 98124  
ATTN: Mr. Roger Wyrick

Lockheed Missiles and Space Co., Inc.  
P. O. Box 1103, W. Street  
Huntsville, AL 35807  
ATTN: Mr. B. H. Shirley

Lockheed Missiles and Space Co., Inc.  
Department 81-10, Bldg. 154  
Sunnyvale, CA 94088  
ATTN: Dr. Lars E. Ericson  
Mr. P. Reding

Nielsen Engineering and Research, Inc.  
510 Clyde Avenue  
Mountain View, CA 94043  
ATTN: Dr. Jack Nielsen (10)

Mr. V. L. Pianta  
P. O. Box 1201  
San Jose, CA 95108

Virginia Polytechnic Institute and  
State University  
Department of Aerospace Engineering  
Blacksburg, VA 24060  
ATTN: Prof. J. A. Schetz  
Prof. A. H. Nayfeh  
Library (2)

North Carolina State University  
Department of Mechanical and  
Aerospace Engineering  
Box 5246  
Raleigh, NC 27607  
ATTN: Prof. F. R. DeJarnette  
Library (2)

University of Tennessee Space Institute  
Tullahoma, TN 37388  
ATTN: Dr. J. M. Wu  
Library (2)

Defense Documentation Center  
Cameron Station  
Alexandria, VA 22314 (12)

Library of Congress  
Washington, DC 20390  
ATTN: Gift and Exchange Division (4)

Defense Printing Service  
Washington Navy Yard  
Washington, DC 20374

LOCAL

E41

G

G20

G23

G30

G40

G41 (Mr. B. Piper, Mr. G. Graff)

K

K02

K04

K05

K20

K21 (Dr. J. Sun, Dr. F. G. Moore) (20)

K22

K23 (Mr. J. Mitchell)

K50

K80 (Mr. S. Hastings)

K81 (Dr. M. Krumins) (2)

K81 (Mr. F. Baltakis)

K82 (Dr. J. Goeller, Dr. N. Sheets,  
Mr. F. Regan)

R

R44 (Dr. J. Solomon)

X210 (2)